Special Report 86-10
May 1986

Revised guidelines for blasting floating ice

Malcolm Mellor

Prepared for
OFFICE OF THE CHIEF OF ENGINEERS

Unclassified

SECURITY CLASSIFICATION OF THIS PAGE *(When Data Entered)*

REPORT DOCUMENTATION PAGE		READ INSTRUCTIONS BEFORE COMPLETING FORM
1. REPORT NUMBER Special Report 86-10	2. GOVT ACCESSION NO.	3. RECIPIENT'S CATALOG NUMBER
4. TITLE *(and Subtitle)* DERIVATION OF GUIDELINES FOR BLASTING FLOATING ICE		5. TYPE OF REPORT & PERIOD COVERED 6. PERFORMING ORG. REPORT NUMBER
7. AUTHOR(s) Malcolm Mellor		8. CONTRACT OR GRANT NUMBER(s)
9. PERFORMING ORGANIZATION NAME AND ADDRESS U.S. Army Cold Regions Research and Engineering Laboratory Hanover, New Hampshire 03755-1290		10. PROGRAM ELEMENT, PROJECT, TASK AREA & WORK UNIT NUMBERS Program Element 6.27.40A DA Project 4A762730AT42 Task Area CS, Work Unit 029
11. CONTROLLING OFFICE NAME AND ADDRESS Office of the Chief of Engineers Washington, D.C. 20314		12. REPORT DATE May 1986 13. NUMBER OF PAGES 43
14. MONITORING AGENCY NAME & ADDRESS(if different from Controlling Office)		15. SECURITY CLASS. *(of this report)* Unclassified 15a. DECLASSIFICATION/DOWNGRADING SCHEDULE

16. DISTRIBUTION STATEMENT *(of this Report)*

Approved for public release; distribution is unlimited.

17. DISTRIBUTION STATEMENT *(of the abstract entered in Block 20, if different from Report)*

18. SUPPLEMENTARY NOTES

19. KEY WORDS *(Continue on reverse side if necessary and identify by block number)*

Cold regions
Explosion effects
Blasting
Ice penetration
Underwater explosions

20. ABSTRACT *(Continue on reverse side if necessary and identify by block number)*

Empirical prediction curves for ice blasting are given, and their derivation and use is explained. Alternative forms of the curves, which relate more closely to conventional underwater explosion technology, are developed and examined. Results of experiments with gas blasting devices are summarized and discussed in relation to the cratering effects of conventional explosives. There is a brief discussion of the energetics of ice fragmentation, effects of surface charges are outlined, and penetration by shaped charges is described. Some test data that were not previously available are given in an appendix.

DD FORM 1 JAN 73 1473 EDITION OF 1 NOV 65 IS OBSOLETE

Unclassified

SECURITY CLASSIFICATION OF THIS PAGE *(When Data Entered)*

PREFACE

This report was prepared by Malcolm Mellor, Research Physical Scientist, of the Experimental Engineering Division, U.S. Army Cold Regions Research and Engineering Laboratory. The work was performed as part of DA Project 4A762730AT42, Design, Construction, and Operations Technology for Cold Regions, Task Area CS, Combat Support, Work Unit 029, Explosives and Projectile Impact Under Winter Conditions.

The author thanks R. Gerard and P. Sellmann for technical review of the manuscript.

CONTENTS

ILLUSTRATIONS

TABLES

DERIVATION OF GUIDELINES FOR BLASTING FLOATING ICE

Malcolm Mellor

Introduction

In 1972, guidelines for blasting floating ice sheets were developed by analyzing all the test data that were then available (Mellor 1972). A decade later, the 1972 curves were revised after addition of new data to the file (Mellor 1982). Since then, a few more data sets have been obtained, and the curves have been updated again.

In developing the original design curves, the primary concern was practical convenience, and certain simplifying assumptions were made. It now appears that these assumptions are adequately justified within broad limits of practical applicability, and the empirical correlations are not improved by more involved treatment of the relevant physics.

One purpose of this paper is to give the current version of the ice-blasting curves, and to describe their use. A second purpose is to explain alternative methods of analysis which may be more correct in terms of physical principles.

Data sources

Most of the data used in 1982 were from obscure or unpublished reports, so all relevant data were tabulated in an appendix to the report (Mellor 1982). Data added to the file since then are from similarly obscure sources, and they are given here in Appendix A. Two tables give results of tests on arctic sea ice that were made in 1960 and 1961 by the U.S. Navy; the data were not available for release until recently. Another table gives some results from tests that were made in Korea by the author subsequent to the 1982 report. In these tests, the emphasis was on pattern charges, but a few single-charge shots were made. Another table covers tests made by the author at a site in the U.S. in 1984. The final tables give some very recent results from Korea (data from Table A5 were not included in the analysis).

When these results were added to the original collection, the file that was analyzed had 312 data sets, compared with 291 in 1982 (315 sets are now available).

Traditional English units were used in the tabulation and analysis of data (App. B), since these units still dominate in North American explosions technology. Final results can easily be converted into SI units.

Scaling of test data for standard curves

To remove the effect of charge size, Hopkinson scaling, or cube root scaling, was adopted from the start. All linear dimensions of the problem are divided by the cube root of charge weight. Although this gives linear dimensions with units of $ft/lb^{1/3}$ or $m/kg^{1/3}$, the lengths are effectively dimensionless, since the cube root of charge weight represents the charge radius for constant explosive density. This type of scaling implies geometric similarity.

Cube root scaling is not strictly valid for underground explosions, where the material strength increases with gravity body forces, nor for underwater explosions, where the static head is the water depth plus a 10-m head representing atmospheric pressure. However, in neither of these situations does cube root scaling distort the results significantly when charge mass ranges from less than 1 kg to more than 1 tonne. To improve the fitting of curves to cratering data or water plume data for certain ranges, empirical exponents smaller than one-third have sometimes been applied to the charge weight that scales either depth, or all linear dimensions. This is inelegant and potentially confusing; it is best avoided if possible.

Alternative normalizing parameters include: (1) charge radius for an equivalent spherical charge of some reference explosive, and (2) the theoretical maximum radius of the underwater gas bubble for the first bubble pulse. These are unsuitable for practical work. The engineer or blaster knows, or can determine, the weight of an explosive charge. By contrast, effective charge radius and maximum bubble radius have to be determined from calculations or conversion charts.

Standard data analysis

To update the basic design curves, the original analytical procedure was followed (Mellor 1972, 1982). Taking scaled charge depth and scaled ice thickness as independent variables X_1 and X_2, the scaled crater radius (dependent variable Y) is first expressed as a 10-term polynomial in X_1

and X_2, with terms and cross-products up to the third power. Assuming all error to be in determination of Y, the 10 coefficients of the regression equation are then determined. The relative significance of each term is examined by stepwise regression, coefficients being deleted successively from t-test values, with successive checks on the multiple correlation coefficient and the standard error of estimate. This has always led to the dropping of the same two terms, b_1 and b_4 of the 10-term polynomial (coefficients for X_1 and X_1X_2). The curves are then drawn from this final 8-term regression equation; Y is plotted against X_1 with X_2 as parameter, and Y is plotted against X_2 with X_1 as parameter (Fig. 1).

For the present collection of data, the standard error of estimate is 1.370 ft/lb$^{1/3}$, or 0.543 m/kg$^{1/3}$ (a deterioration from the 1982 value of 1.265 ft/lb$^{1/3}$ or 0.502 m/kg$^{1/3}$) and the multiple correlation coefficient r = 0.708 (almost the same as the 1982 value of 0.707). The 8-term regression equation in units of ft and lb was:

$$Y = 5.222 + 3.208\ X_2 - 0.1273\ X_1^2 - 2.242\ X_2^2 + 0.006870\ X_1^3 + 0.02191\ X_1^2X_2 - 0.07376\ X_1X_2^2 + 0.3627\ X_2^3$$

Effects of explosive type and ice type

With only a limited amount of data, it is not feasible to consider the variation of explosive type, or of ice type, in the regression analysis.

The specific energy of typical explosives varies within fairly narrow limits, and there is appreciably less variation in the cube root of the charge yield that is used for scaling linear dimensions (typically $< \pm 9\%$). Only a small proportion of the total energy goes into shock propagation, and therefore changes in that proportion relative to the energy for gas expansion are not of major significance. In 1982 the data were examined carefully for signs of systematic variation attributable to explosive type, but there was no conclusive evidence of such an effect. Since then, it has been found that gas blasting devices produce much the same ice-breaking effects as energetically equivalent charges of high explosive (Mellor 1984a), so it seems likely that variation of explosive characteristics is not of major significance when the degree of fragmentation is not of great concern.

Data for underground explosions show that crater dimensions in a semi-infinite solid are rather insensitive to material properties for a wide range of rocks and soils, and this suggests that minor variation of ice

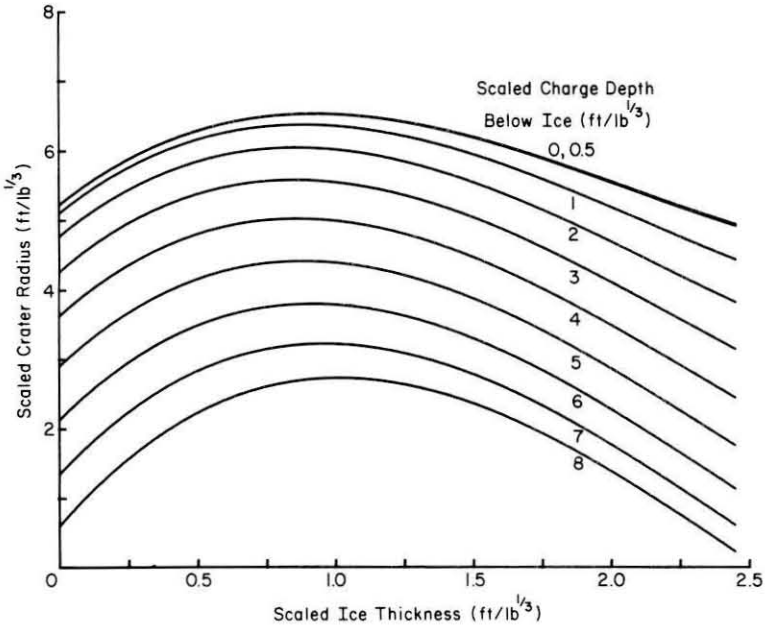

a. Scaled crater radius as a function of scaled ice thickness, with scaled charge depth as parameter.

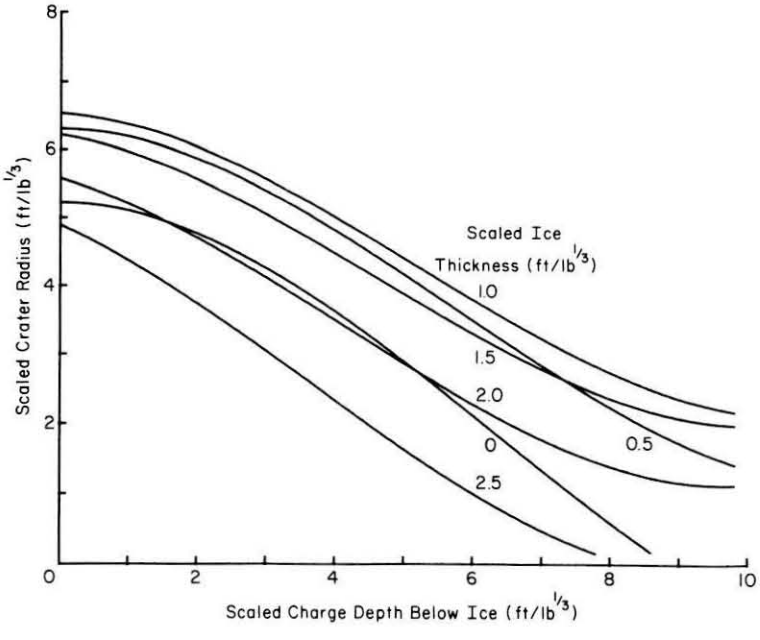

b. Scaled crater radius as a function of scaled charge depth, with scaled ice thickness as parameter.

Figure 1. Design curves for ice blasting.

properties may have little effect on craters in ice. In a previous report (Mellor 1982), it was suggested that the thickness of a snow cover on floating ice might have more significance than variation in ice properties.

Interpretation and application of design curves

The standard curves are generated in traditional English units for use in the U.S. Equivalent SI plots can be produced by suitable choice of intervals for the parameter, but there is no real need if appropriate conversion factors are used in working a problem. To convert $ft/lb^{1/3}$ to $m/kg^{1/3}$, multiply by 0.3967; to convert $m/kg^{1/3}$ to $ft/lb^{1/3}$, multiply by 2.5208. For m-ft and kg-lb conversion, the factors are 3.281 and 2.205 respectively.

Figure 1 shows that maximum crater diameter, or area, is achieved with a scaled charge depth of 0 to 0.5 $ft/lb^{1/3}$ (0 to 0.2 $m/kg^{1/3}$) below the base of the ice cover, provided that the scaled ice thickness is around 0.9 $ft/lb^{1/3}$ (0.36 $m/kg^{1/3}$). In other words, the best results are obtained with the charge almost in contact with the base of the ice. With these optimum conditions, the scaled crater radius is 6.56 $ft/lb^{1/3}$ (2.6 $m/kg^{1/3}$). The predicted scaled crater diameter is thus just over 13 $ft/lb^{1/3}$ (5.2 $m/kg^{1/3}$), or about 15 times the ice thickness (Fig. 2).

For scaled charge depths greater than 0.5 $ft/lb^{1/3}$ (0.2 $m/kg^{1/3}$), scaled crater radius decreases for all values of scaled ice thickness (Fig. 1). At these greater charge depths, the optimum value of scaled ice thickness appears to vary somewhat.

When using the curves, the usual input is a measured or estimated value of the ice thickness t. If the intent is to get the biggest crater for the least amount of explosive, an optimum charge weight W_{opt} can then

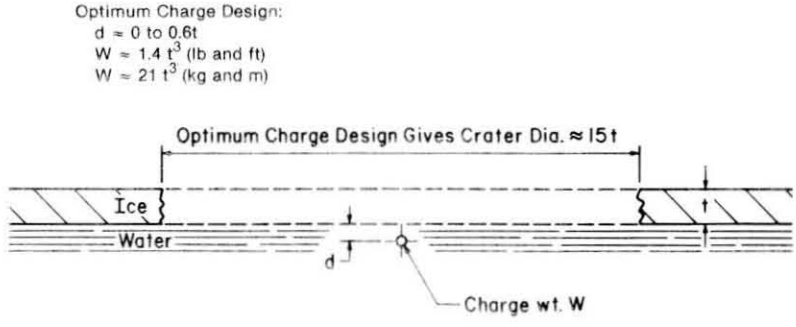

Figure 2. Simple guidelines for optimum charge design (single crater).

be estimated from the optimum ice thickness, which is approximately 0.9 $ft/lb^{1/3}$ (or 0.36 $m/kg^{1/3}$):

$$t/W_{opt}^{1/3} \approx 0.9 \text{ ft/lb}^{1/3}$$

or

$$W_{opt} \approx (t/0.9)^3 \text{ lb} \approx 1.4t^3 \text{ lb}$$

when t is in ft. If t is in m, then

$$W_{opt} \approx (t/0.36)^3 \approx 21t^3 \text{ kg}.$$

The optimum charge depth $d_c/W^{1/3}$ is 0 to 0.5 $ft/lb^{1/3}$ (0-0.2 $m/kg^{1/3}$), so that

$$d_c \approx 0 - 0.6t.$$

The easiest rule-of-thumb for predicting the diameter D of an optimum crater is to take

$$D \approx 15t.$$

With ice thickness given, the curves can provide predictions of crater size for non-optimum charge weight and/or charge depth, or they can be used to determine the size of charge needed to produce a crater of specified diameter from a given charge depth. Alternatively, the optimum or maximum thickness of ice can be calculated when charge size and charge depth are specified. These various applications have been illustrated by means of worked numerical examples (Mellor 1982).

Multiple charges for ice breaking

A row of under-ice charges can be used to break a channel, and a multi-row array can be used to fracture ice over a broad area. To design a row, or an array, of ice-breaking charges, it is convenient to first calculate the crater radius R_{c1} for a single charge and then to relate R_{c1} to the spacing s for charges in a row or in a square network.

In a single row of charges where s/R_{c1} is greater than about 2.5, or in an array where $s/R_{c1} > 4$, each charge produces a separate eruption and a separate crater (see Table 1 for references). When s/R_{c1} becomes somewhat smaller than these values, each charge still gives a separate eruption (Fig. 3b-g), but as the ice debris and the water columns fall back again, the ice between the individual craters is subjected to impact, base surge, and violent wave action (Fig. 3 h-m). This can fracture the ice between the craters with varying degrees of fragmentation, depending on s/R_{c1}.

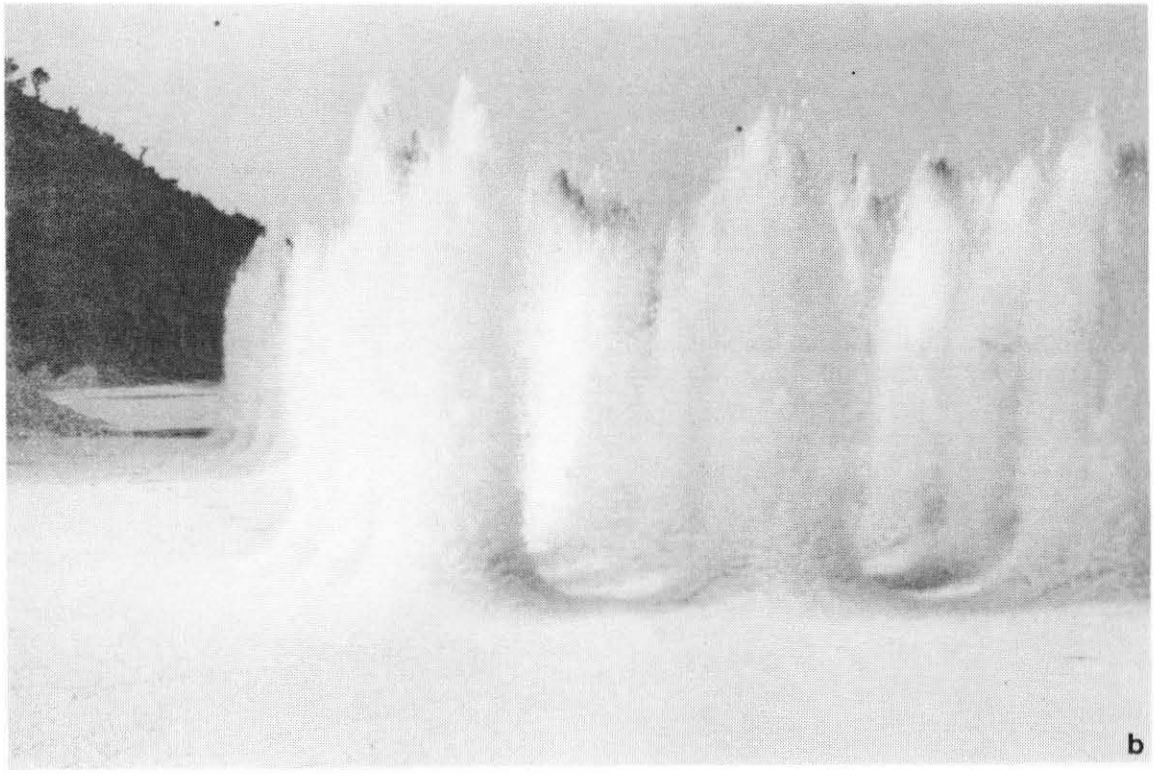

Figure 3. An array of multiple charges breaking through thin ice (5-lb charges on 27-ft centers). Charge depth 0.45 bubble radii. Photos in this sequence were taken at intervals of approximately 0.2 s.

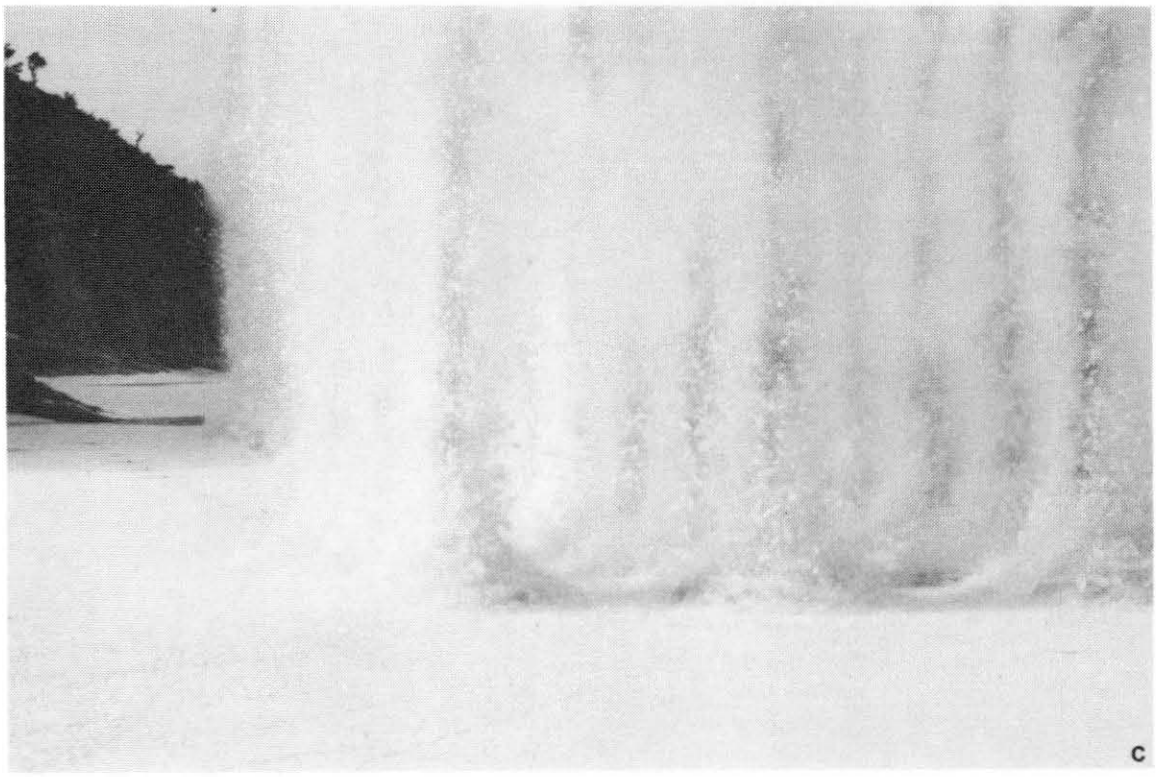

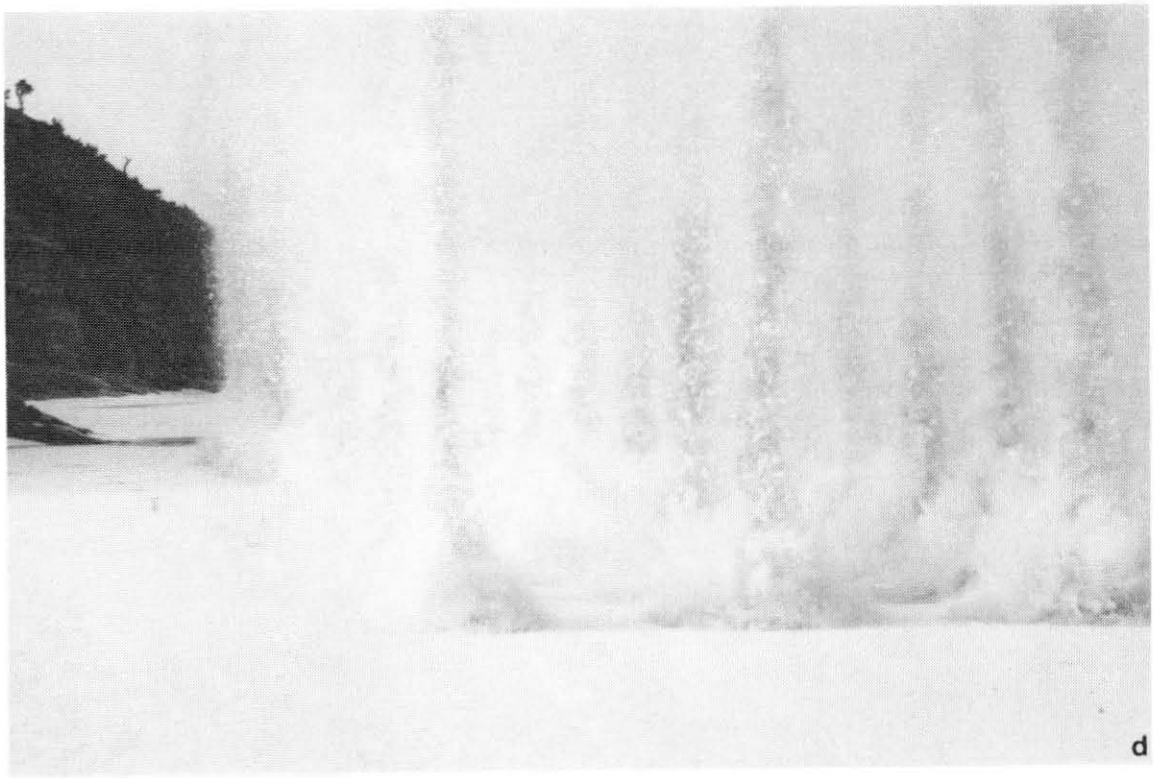

Figure 3 (cont'd). An array of multiple charges breaking through thin ice (5-lb charges on 27-ft centers). Charge depth 0.45 bubble radii. Photos in this sequence were taken at intervals of approximately 0.2 s.

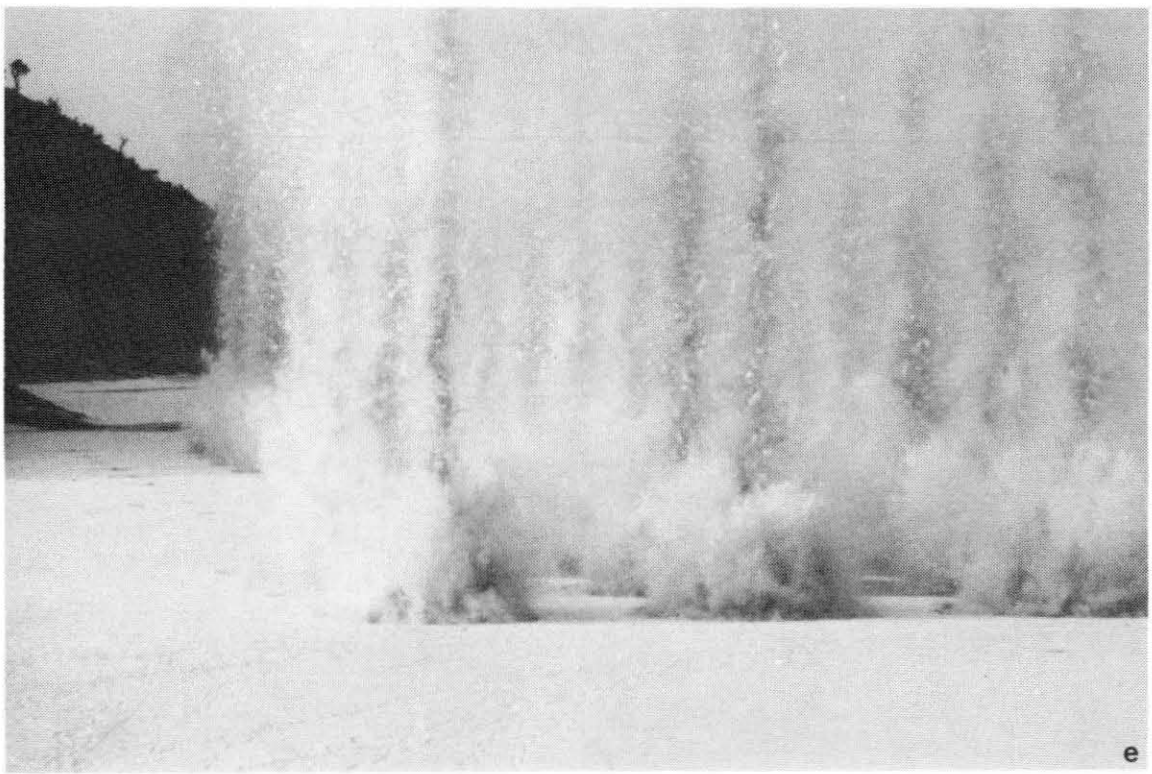

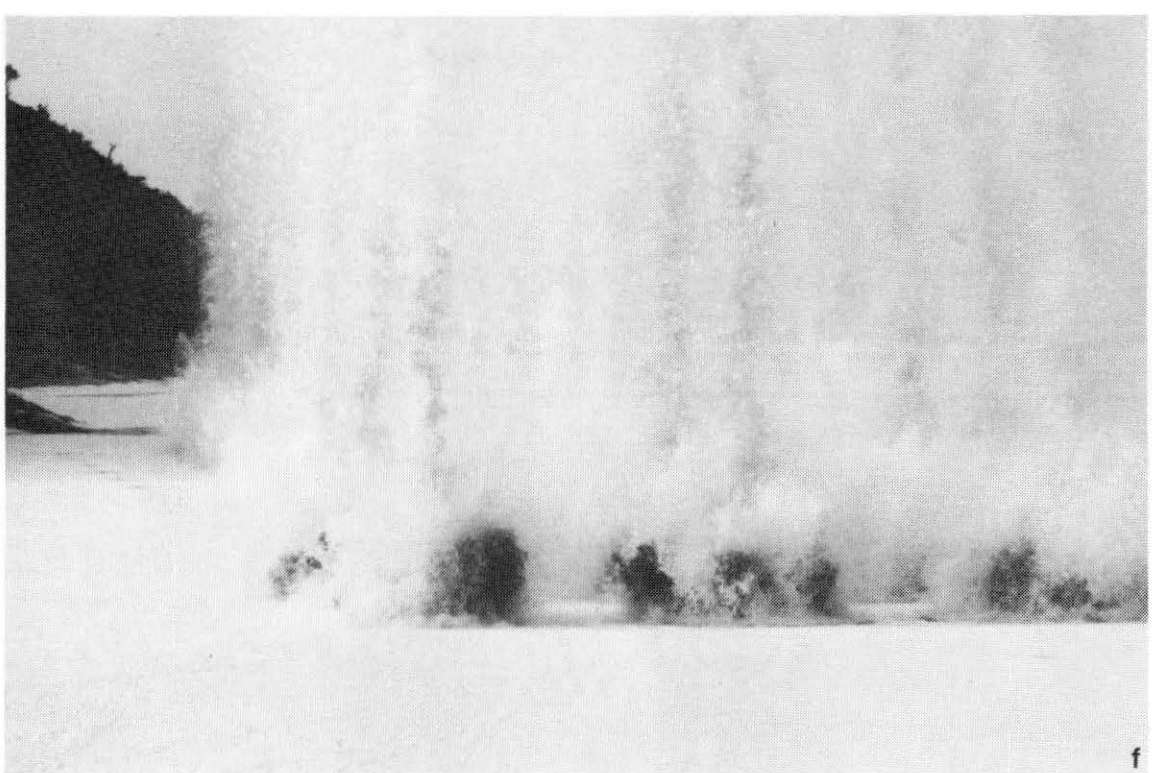

Figure 3 (cont'd).

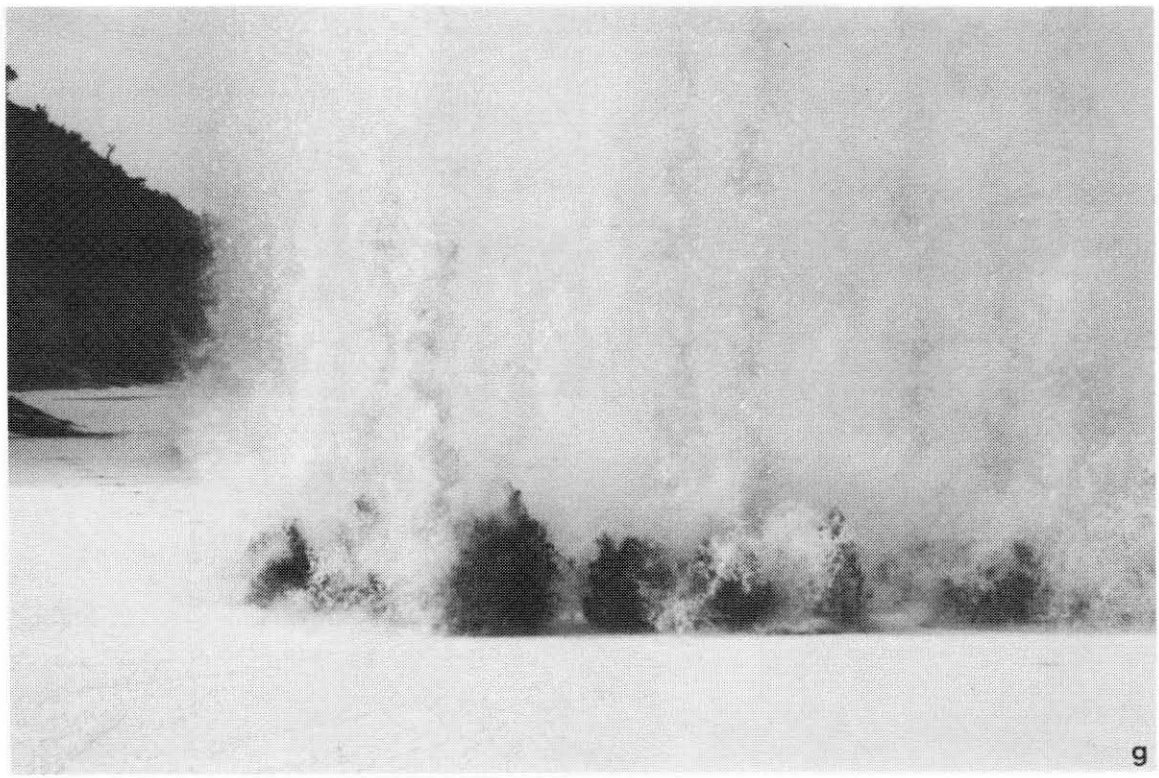

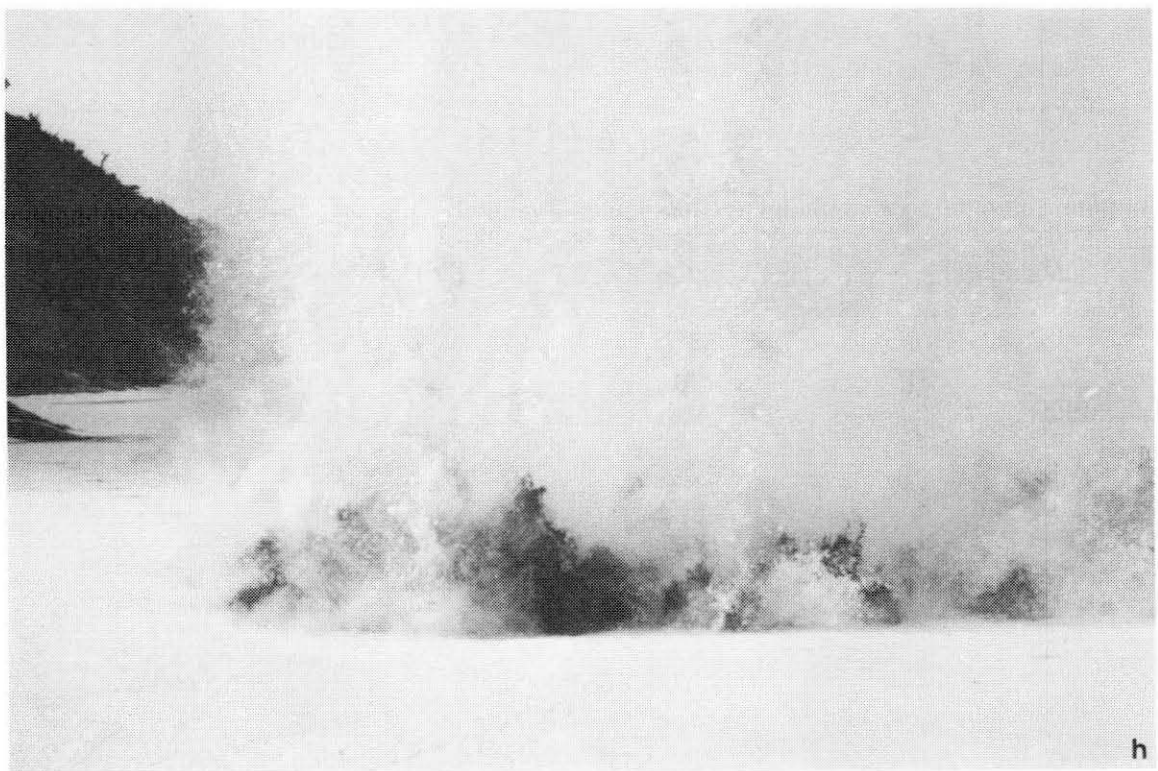

Figure 3 (cont'd). An array of multiple charges breaking through thin ice (5-lb charges on 27-ft centers). Charge depth 0.45 bubble radii. Photos in this sequence were taken at intervals of approximately 0.2 s.

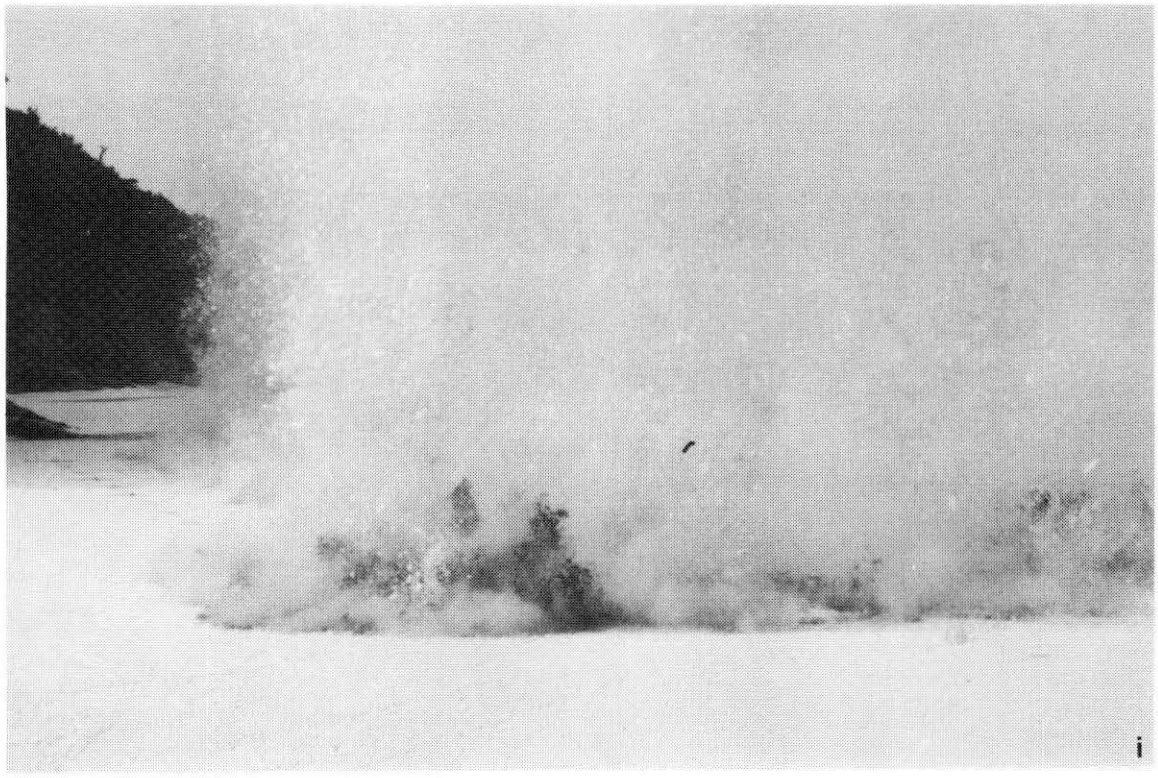

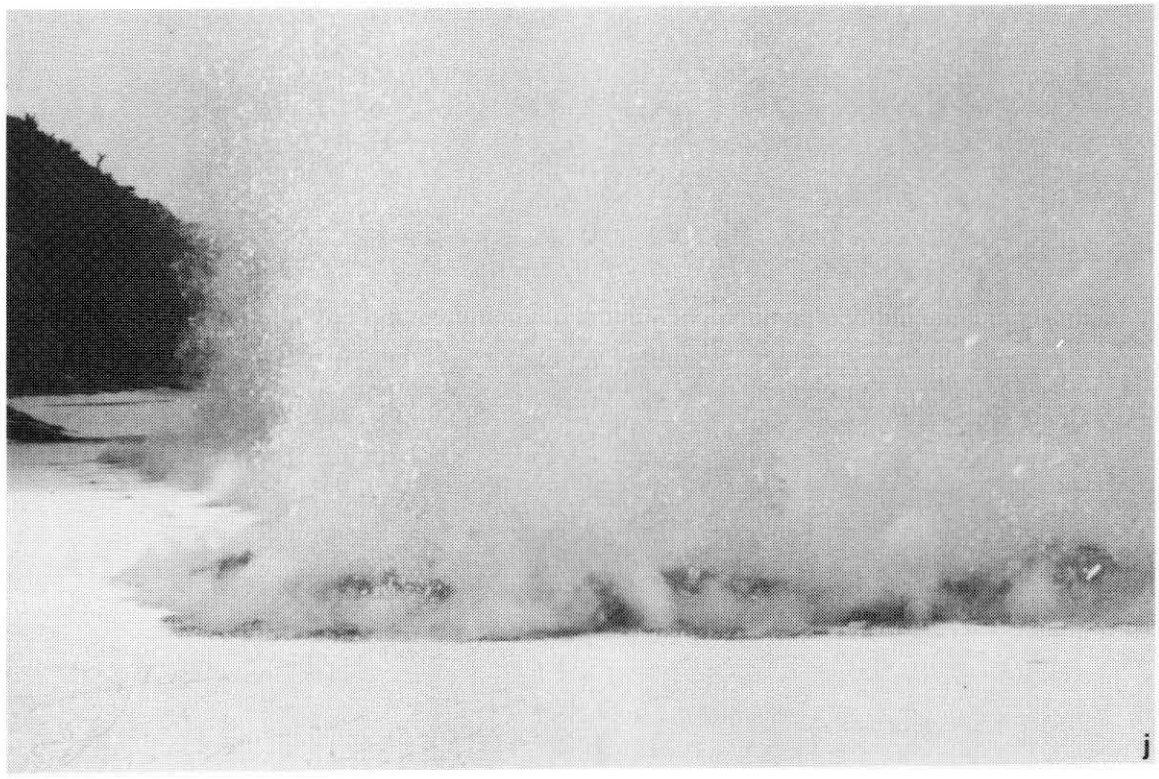

Figure 3 (cont'd).

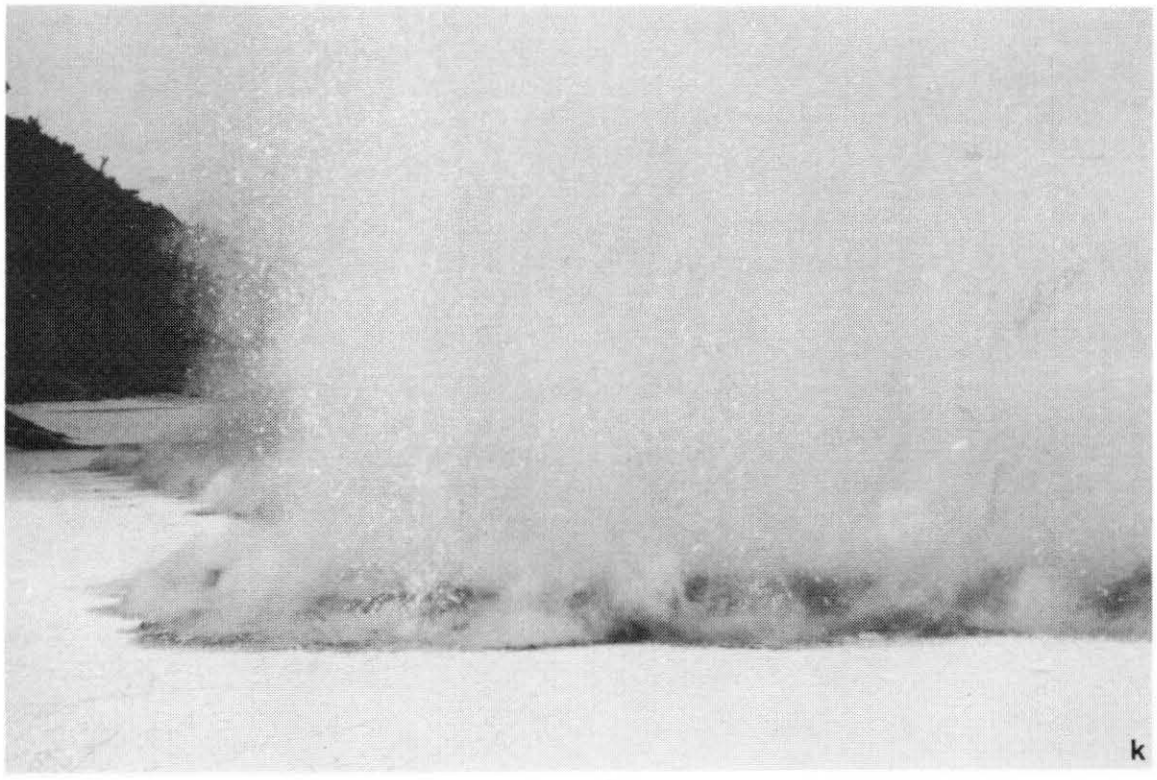

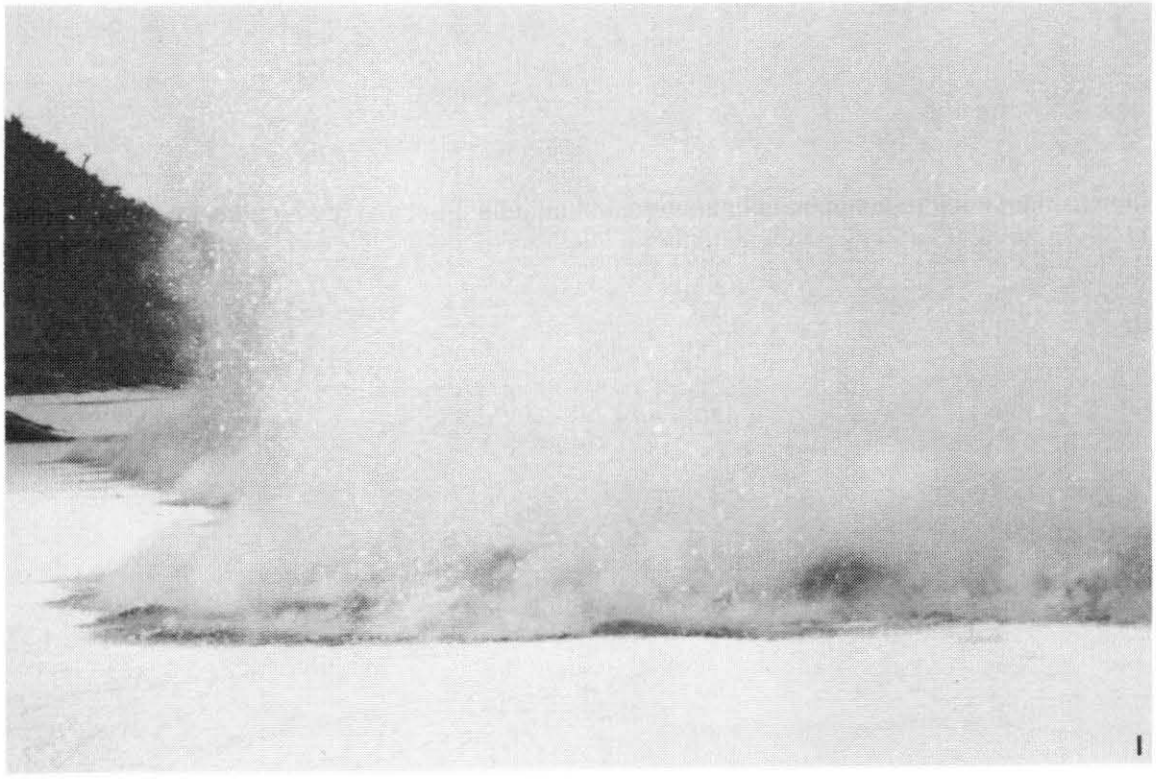

Figure 3 (cont'd). An array of multiple charges breaking through thin ice (5-lb charges on 27-ft centers). Charge depth 0.45 bubble radii. Photos in this sequence were taken at intervals of approximately 0.2 s.

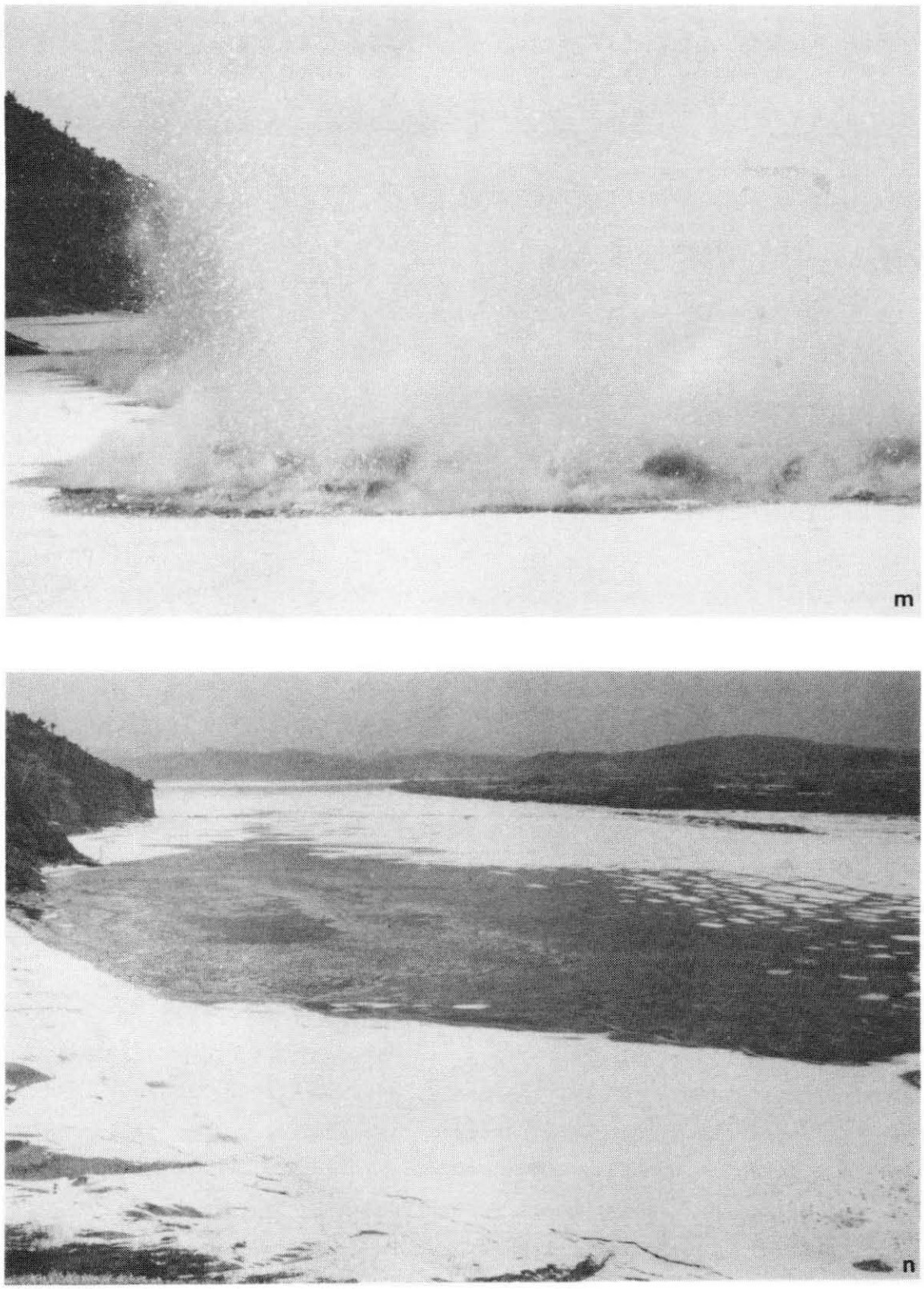

Figure 3 (cont'd).

Table 1. Effects of charges in a single row when each charge is close to optimum for the prevailing ice thickness, and charge depth is about 1t to 1.5t. Based on tests by Kurtz et al. (1966), Fonstad and Gerard (1985) and unpublished work by the author.

Charge spacing	Approximate width of fractured channel, b		
(s/R_{c1})	(b/R_{c1})	(b/s)	Fragmentation
>2.5	Individual craters		As for single crater.
2	3.8	1.9	Poor at edges of channel and in cusps between craters.
1.5	3.4	2.3	Good in mid-channel, less along edges.
1.0	3.4	3.4	Good.

Under these conditions, the author has chosen to accept 1 $ft/lb^{1/3}$ (0.4 $m/kg^{1/3}$) as optimum charge depth (instead of 0-0.5 $ft/lb^{1/3}$) in order to increase the base diameter of the water plume. There are no systematic data to support this judgment, which derives from findings for explosions beneath ice-free surfaces (see Mellor 1986).

Drawing upon limited field data, probable effects of row charges are indicated in Table 1. The charges interact to produce a continuous broken channel when $s/R_{c1} < 2.5$. Fragmentation improves and becomes more uniform as s/R_{c1} decreases, until the row of individual charges approximates the effect of a continuous linear charge, for which the blast effects spread cylindrically rather than spherically.

A multi-row array produces more interference between craters, and the charge spacing can be wider than it is in a single row. The logical charge pattern is a square net of mesh size s. A "diamond," or "5-spot," pattern is obtained by rotating the reference axes of a square mesh through 45°. Limited personal experience with charge arrays indicates that individual craters are formed with $s/R_{c1} > 4$, continuous fracture occurs with $s/R_{c1} = 3$, adequate fragmentation* is obtained with $s/R_{c1} = 2.7$, spacing is somewhat closer than necessary with $s/R_{c1} = 2.3$, and spacing is wastefully close with $s/R_{c1} = 2$. Fonstad and Gerard (1985) deduced an

*More or less equant fragments, as distinct from slab fragments.

upper limit for useful interference as $s/R_{c1} = 3.5$, which agrees reasonably well with a value of 3.8 suggested earlier (Mellor 1982).

Charge design for thin ice

If the ice is thin (<1 ft, <0.3 m), the optimum size of a single charge is small, and the absolute diameter of the resulting crater is also small (<15 ft, <4.5 m). When the objective is to break a wide channel or a broad area in thin ice with multiple charges, the required number of optimum charges may be large. Under these circumstances, the effort involved in drilling and charge placement can become excessive, and it may be more efficient in practical terms to use charges that are bigger than optimum, and to set them further apart.

Having made the calculations for optimum charge size to get a feel for things, a guess can be made at the total amount of explosive that seems affordable for the job, and a new charge size can be estimated (e.g. 5 lb instead of 1 lb, or 2.5 kg instead of 0.5 kg). The scaled ice thickness for the new charge weight is then calculated, and the curves of Figure 1 are used to obtain the corresponding value of R_{c1} (perhaps taking a scaled charge depth of about 1 ft/lb$^{1/3}$ or 0.4 m/kg$^{1/3}$, as suggested earlier). Using the chosen value of s/R_{c1}, say 2.7, the new value of charge spacing s is obtained.

Specific energy, or powder factor, for ice fragmentation

The specific energy for fragmentation of a solid, E_s, is the energy consumed to break unit volume. The energy in a charge of weight W is kW, where k is a characteristic specific energy content for the particular explosive. k can be taken either as the heat of explosion, typically around 4.2 to 4.8 kJ/g for high explosives, or as the gas expansion energy, which is roughly 20% of the heat of explosion. The volume of ice broken by a single charge is $R_c\ t$, where R_c is crater radius and t is ice thickness. Thus, for explosive icebreaking,

$$E_s = \frac{kW}{\pi R_c^{\,2} t} = \frac{k/\pi}{(R_c/W^{1/3})^2\ (t/W^{1/3})}.$$

The weight of explosive per unit volume of fragmented material is known as the powder factor F_p, or as the specific charge. For ice blasting with a single charge:

$$F_p = \frac{W}{\pi R_c^{\,2} t} = \frac{1}{\pi(R_c/W^{1/3})^2\ (t/W^{1/3})}.$$

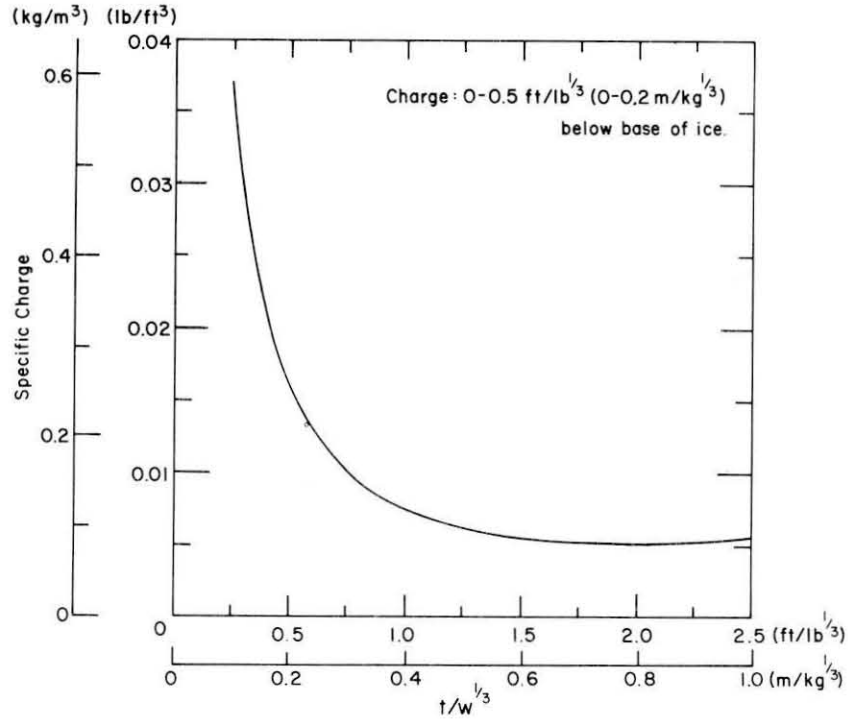

Figure 4. Specific charge, or powder factor, as a function of scaled ice thickness when single charges are at optimum depth.

Figure 4 gives the specific charge (powder factor) as a function of scaled ice thickness for single charges at optimum depth, i.e. immediately below the bottom of the ice. The minimum value of specific charge is 0.0051 lb/ft^3, or 0.082 kg/m^3, and it is obtained when the scaled ice thickness is about 2 ft/lb$^{1/3}$, or 0.8 m/kg$^{1/3}$. In other words, the maximum specific volume of fragmentation occurs with $t/W^{1/3} \approx 2$ ft/lb$^{1/3}$ (0.8/m kg$^{1/3}$), whereas maximum specific area of fragmentation occurs with $t/W^{1/3} \approx 0.9$ ft/lb$^{1/3}$ (0.36 m/kg$^{1/3}$).

For comparison, the powder factor for optimum crater blasts in semi-infinite ice is about 0.01 to 0.02 lb/ft^3, or 0.004 to 0.008 kg/m^3.

Values of specific energy E_s for explosive icebreaking by single charges can be obtained from Figure 4 by multiplying values of specific charge by either the heat of explosion or the energy of gas expansion for explosive. The units of this specific energy are energy per unit volume, which reduces to the dimensions of a stress. If we take the heat of explosion as 4.6 kJ/g (1.1 kcal/g), which is about right for TNT, the minimum overall specific energy for explosive icebreaking is about 0.38 MJ/m^3, which is equivalent to 0.38 MPa (55 lbf/in.^{2}). This is comparable to the

specific energy of a fairly large icebreaker (10,000-50,000 hp) when E_s is based on shaft horsepower. The "process specific energy" for a ship, based on propeller thrust and speed, is lower, but this should be compared with an explosive specific energy that is based on the work of gas expansion (about 20% of the value given above).

The specific energy for maximum crater area is obtained by taking $R_c/W^{1/3} = 6.56$ ft/lb$^{1/3}$ and $t/W^{1/3} = 0.9$ ft/lb$^{1/3}$. These give $F_p = 0.0082$ lb/ft^3 (0.13 kg/m^3) and, with $k = 4.6$ kJ/g, $E_s = 0.6$ MJ/m^3 (0.6 MPa, 88 lbf/in.^{2}). If specific energy is based on the work of gas expansion, $E_s \approx 0.12$ MJ/m^3. These values are a bit higher than corresponding values for maximum specific volume of broken ice, but are still comparable to the specific energy for an icebreaking ship.

Other analytical schemes

In practical ice blasting, charge depth has usually been referred to the base of the ice sheet, and test data have been reported accordingly. However, in underwater explosion technology, the water surface is the obvious datum for charge depth, and it can be argued that it is also a logical datum for charge depth in ice blasting. To convert traditional charge depth to charge depth below water level, we simply add the ice thickness multiplied by the specific gravity of the ice. Having made this conversion, the regression analysis can be repeated to give a prediction of scaled crater radius as a function of scaled ice thickness and scaled charge depth below water level.

Figure 5 gives the prediction curves when water level is the reference for charge depth. The curves are broadly similar to the standard curves, but they necessarily cut off for the portions where depth is less than the ice thickness. The predictions are essentially the same as those given by the standard curves. However, the empirical correlation is not as good as it is for the standard curves. The standard error of Y is 1.408 ft/lb$^{1/3}$, compared with 1.370 ft/lb$^{1/3}$. The multiple correlation coefficient r is 0.684, compared with 0.708 for the standard curves.

In Figure 5b the ice cratering behavior is compared with the types of surface eruptions which would occur at an ice-free surface. The maximum scaled crater radius is achieved when charge depth is in the shallow end of the range which produces columnar eruptions from a free surface.

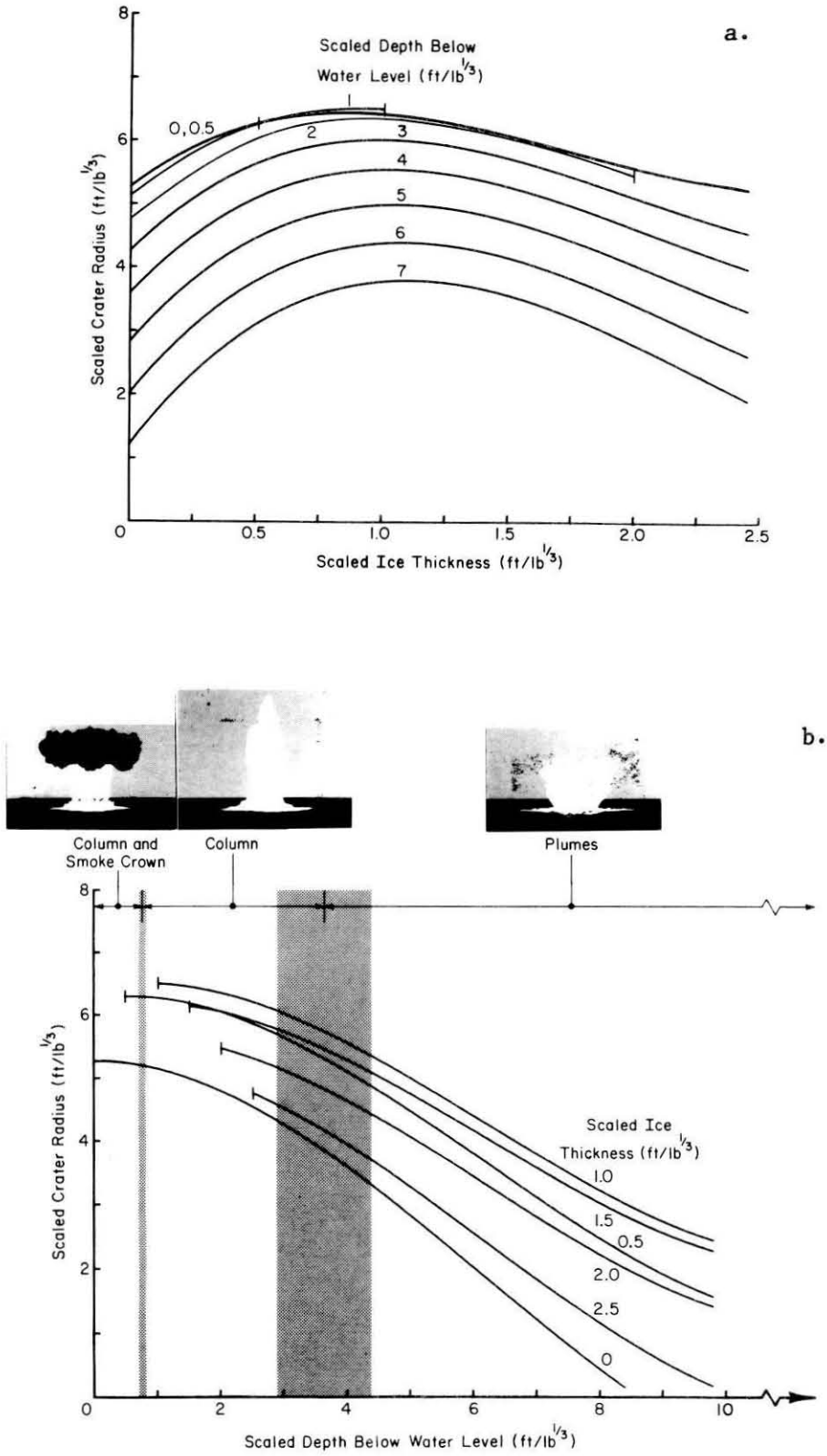

Figure 5. Prediction curves derived from regression analysis when the datum for charge depth is the level of the water surface.

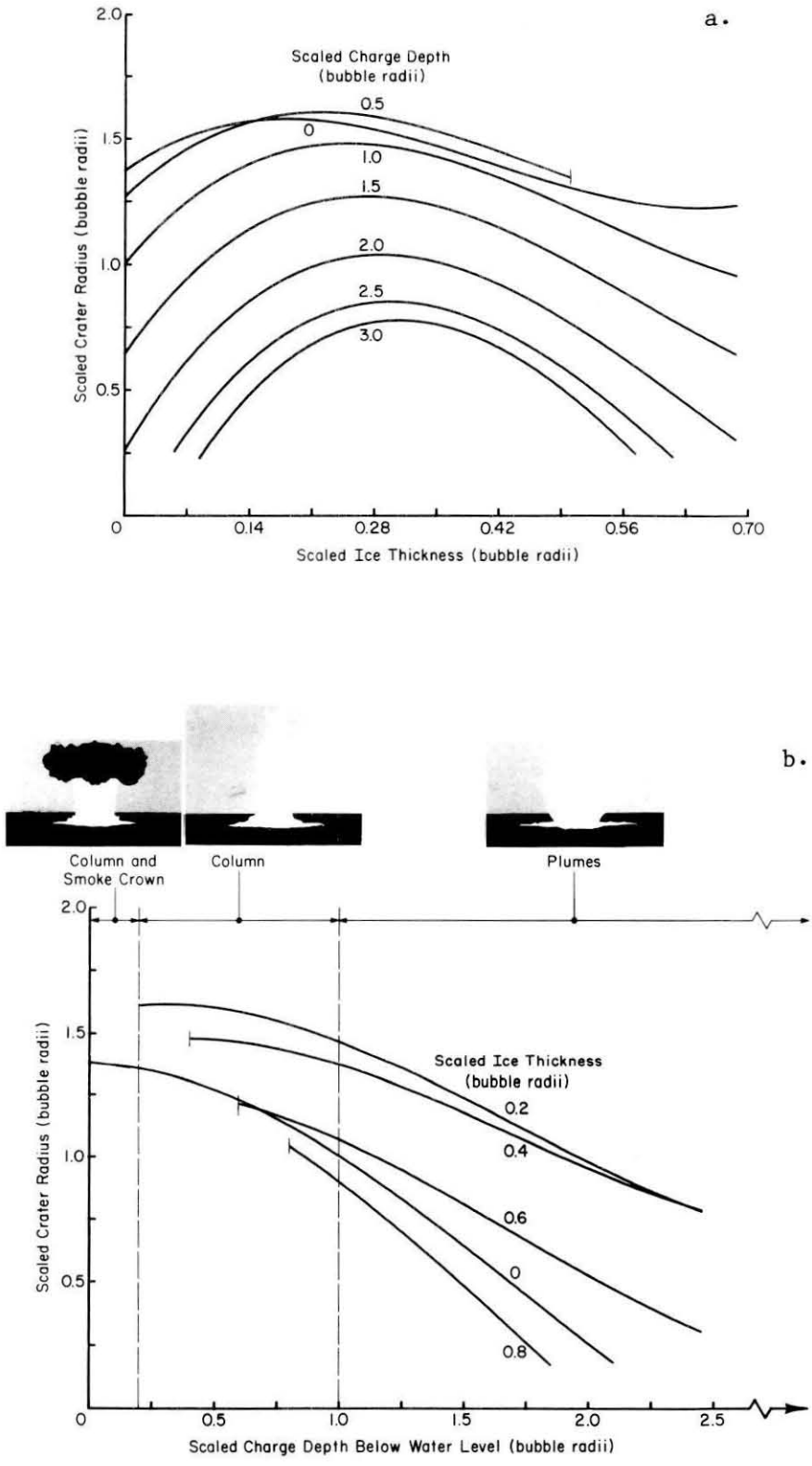

Figure 6. Prediction curves derived from regression analysis when linear dimensions are scaled with respect to maximum bubble radius, and water level is the depth datum.

In underwater explosion technology, linear dimensions are sometimes scaled with respect to the theoretical maximum radius of the gas bubble for the first pulse, R_{bm}. This procedure is particularly useful in dealing with problems that involve surface effects, such as eruption of waterspouts. Using standard relations which give R_{bm} as a function of charge weight and depth below the water surface (see Mellor 1986), the data for ice blasting can be converted into dimensionless form, such that all linear dimensions are normalized with respect to R_{bm}. The data were scaled in this way, using water level as the depth datum, and the regression analysis was repeated.

Results of the regression analysis for the bubble-scaled data are shown in Figure 6. The predictions are more or less the same as those of the standard curves, but the empirical correlation is not as good. The multiple correlation coefficient r is 0.649, compared with 0.708 for the standard curves and 0.684 for cube-root data referred to water level. In Figure 6b the depth ranges for various types of free-surface eruptions are shown. As before, it can be seen that the scaled crater radius is a maximum when charge depth is in the range that produces columnar waterspouts in ice-free conditions.

For practical use, there is no doubt that the standard curves are more convenient, and slightly more reliable, than the alternative forms described here. However, the bubble-scaled curves provide some insight into the relation between ice cratering and underwater gas bubbles. The maximum scaled crater radius that can be achieved is about 1.63 R_{bm}, and it is obtained when the charge depth and the ice thickness are only about 0.3 R_{bm}. This implies that water driven by the expanding gas bursts through the ice during the first bubble expansion (Fig. 7).

Gas blasting

Floating ice can be broken by a rapid gas discharge beneath the ice. Tests have been made with a variety of systems, all of which discharge at relatively low pressure without propagating a true shock (Mellor 1984a). Experimental equipment has included: (a) carbon dioxide shells (discharge pressure 70-90 MPa), (b) an airblasting system (69-83 MPa), (c) an air gun (17 MPa), and (d) a fuel/air combustion system (2.3-4.3 MPa).

Gas blasting results cannot be compared directly with explosives data. To draw any kind of conclusions from the limited gas blasting data,

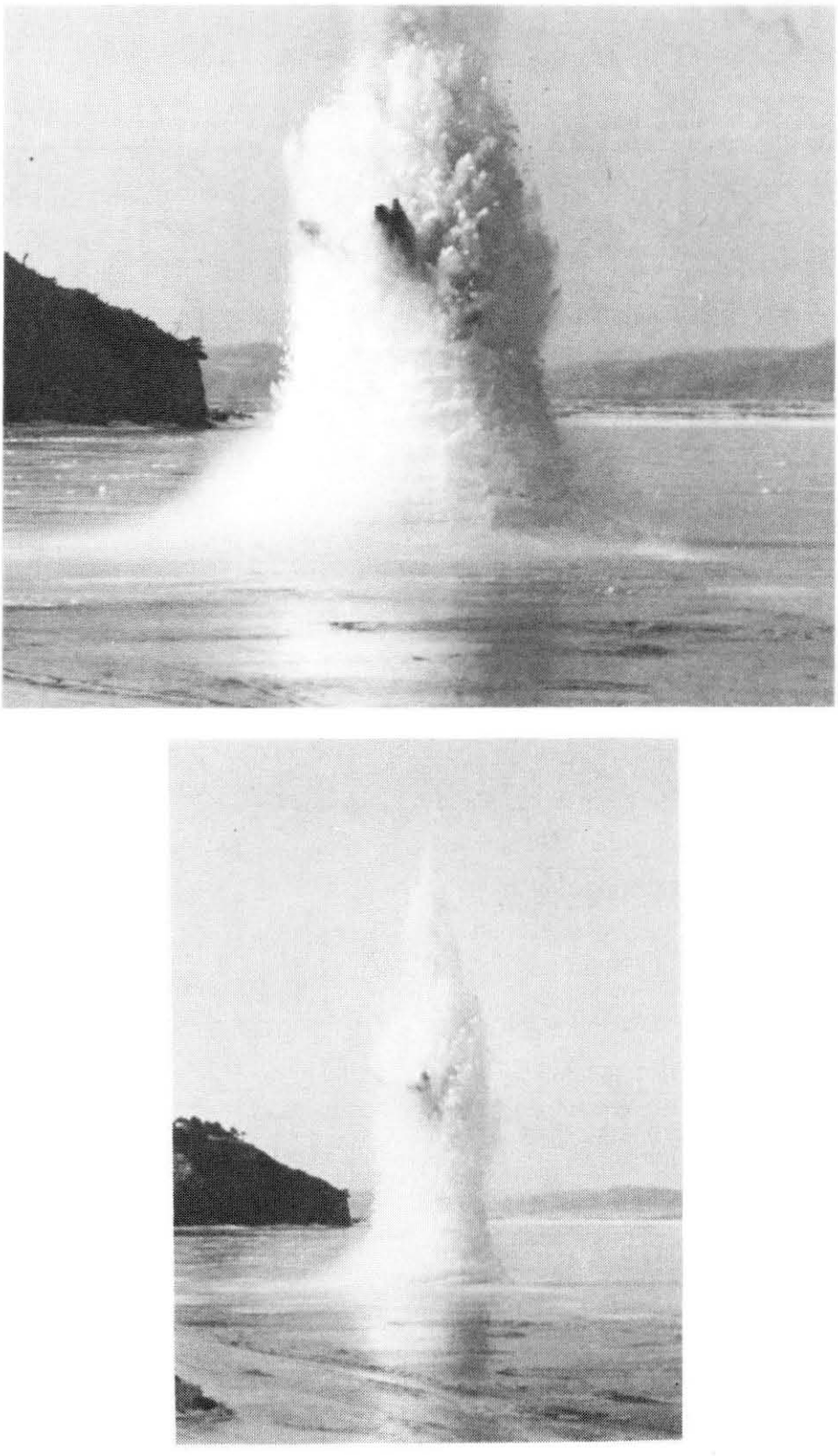

Figure 7. Eruption through very thin ice. Charge depth below water level is 0.49 bubble radii. The form of the eruption is a column with a center jet.

dimensions have to be scaled with respect to the cube root of the discharge energy, which is taken as the energy for adiabatic gas expansion to atmospheric pressure. For comparison with explosives, it is not clear whether the energy of the explosive should be taken as the heat of explosion or as the energy of gas expansion. If a scaled dimension for gas blasting has units of $m/MJ^{1/3}$, it can be converted to units of $m/kg^{1/3}$ by multiplying by the cube root of an explosive specific energy factor that has units of MJ/kg. For TNT, the heat of explosion is approximately 4.56 MJ/kg and the energy of gas expansion is 0.87 MJ/kg; the corresponding cube root factors are 1.66 and 0.955 $(MJ/kg)^{1/3}$.

For ice-breaking gas discharges of magnitude 1 MJ, optimum scaled ice thickness for maximum crater diameter is about 0.4 $m/MJ^{1/3}$, optimum charge depth is in the range 0 to 0.6 $m/MJ^{1/3}$, and the resulting maximum crater radius is about 2.9 $m/MJ^{1/3}$ (Mellor 1984a). If the gas expansion conversion factor for high explosives is applied to the optimum crater results for explosives (Fig. 1), the corresponding values are: optimum ice thickness 0.38 $m/MJ^{1/3}$, optimum charge depth 0 to 0.21 $m/MJ^{1/3}$, and maximum crater radius 2.7 $m/MJ^{1/3}$. Considering all the uncertainties that are involved, this is remarkably close agreement between gas blasting and explosives blasting. Furthermore, both gas blasting and explosives give a probable maximum value for the scaled crater diameter of approximately 15 times the optimum ice thickness.

The specific energy E_s for maximum values of scaled crater diameter is about 0.1 MJ/m^3. This is the same as the corresponding specific energy for conventional explosives when E_s is based on the work of gas expansion rather than upon the heat of explosion ($E_s \approx 0.12$ MJ/m^3).

This suggests that, for optimum cratering, the crater size is controlled by gas expansion and water displacement, not by shock propagation. Since most of the energy of a high explosive goes into gas expansion, and since the energy per unit mass of typical explosives does not vary between very wide limits, it also seems reasonable to expect that optimum crater dimensions will be fairly insensitive to explosive type.

If crater size is influenced mainly by gas expansion and water displacement, then variations in ice type might not have much effect. In particular, an ice cover formed by accumulation of ice fragments might respond much like an intact ice plate.

Charges on, or within, the ice sheet

A small charge placed on top of a thick ice sheet, or in its upper half, has much the same effect as a cratering charge in semi-infinite ice (Fig. 8). Figure 9 summarizes the data for scaled dimensions of the true crater in deep ice. The true crater is the more or less conical region of fractured ice, as distinct from the apparent crater, which is the visible open hole. The maximum scaled radius of the true crater, measured at the ice/air surface, is in the range 3 to 5 ft/lb$^{1/3}$ (1.2 to 2.0 m/kg$^{1/3}$). This maximum is achieved with a scaled charge depth of 3 to 4 ft/lb$^{1/3}$ (1.2 to 1.6 m/kg$^{1/3}$).

Corresponding data for the apparent crater are given in Figure 10. Dimensions of the apparent crater are smaller than those of the true crater because some of the fractured ice is not grossly displaced, and some ejected fragments fall back into the crater.

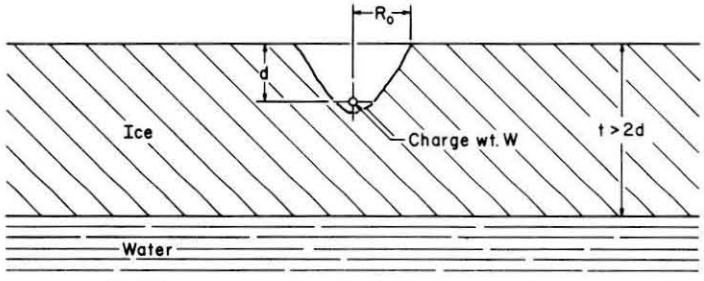

For Optimum Charge Depth:
$d = d_{opt} \approx 4W^{1/3}$ (ft and lb)
$\approx 1.6^{1/3}$ (m and kg)
$R_o \approx d$

For Zero Charge Depth:
$d = 0$
$R_o/W^{1/3} \approx 2-3$ (ft and lb)
$\approx 0.8-1.2$ (m and kg)

Below Critical Charge Depth:
$d/W^{1/3} > 4.3$ (ft and lb)
> 1.7 (m and kg)
$R_o = 0$

Figure 8. Summary of dimensions for the true crater produced by a small charge inside thick ice.

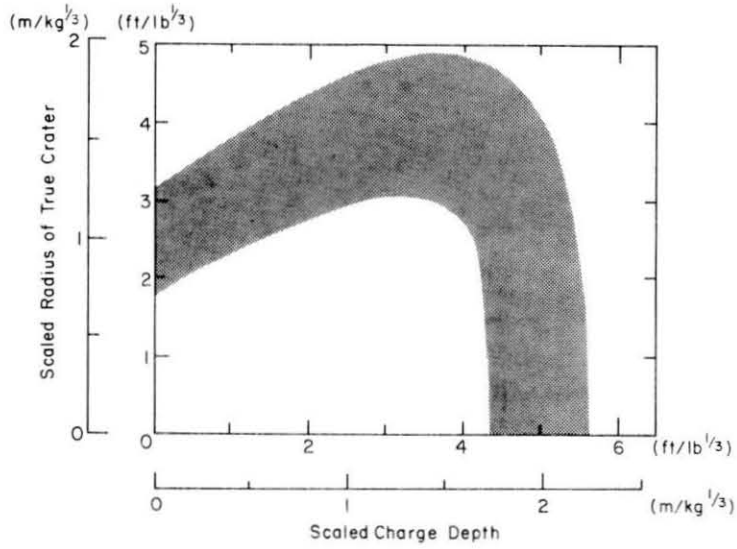

a. Scaled crater radius as a function of scaled charge depth.

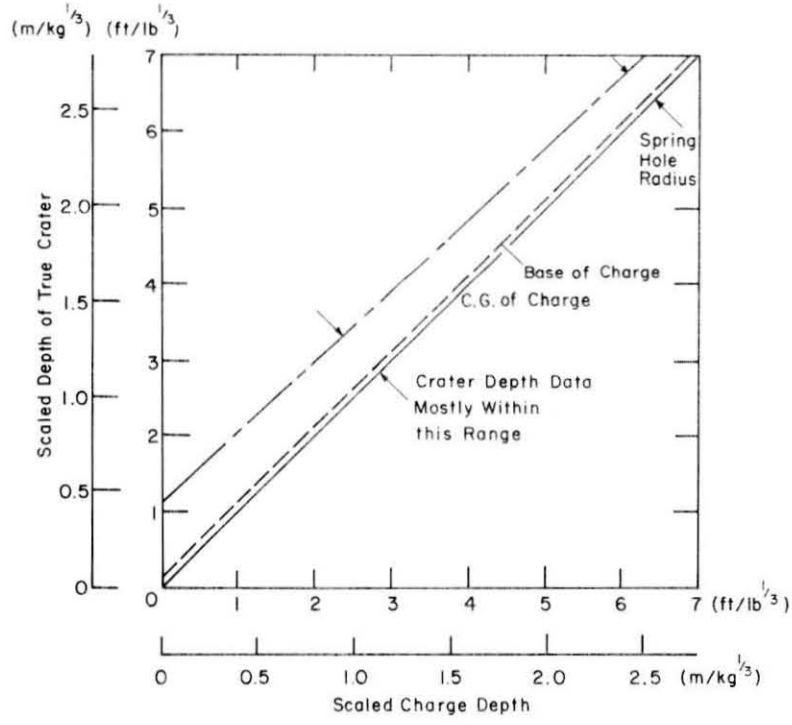

b. Scaled crater depth as a function of scaled charge depth.

Figure 9. Summary of data for the scaled dimensions of the true crater in massive ice. (Data from Livingston 1960.)

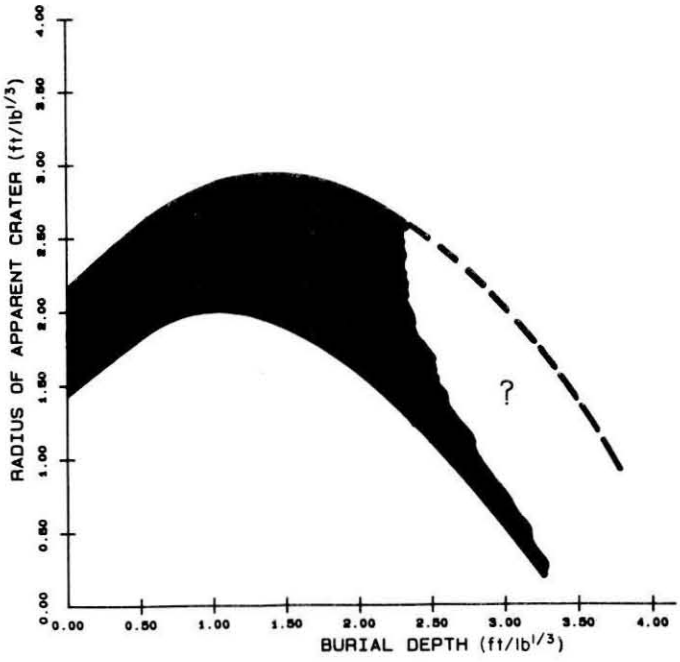

a. Scaled crater radius as a function of scaled charge depth.

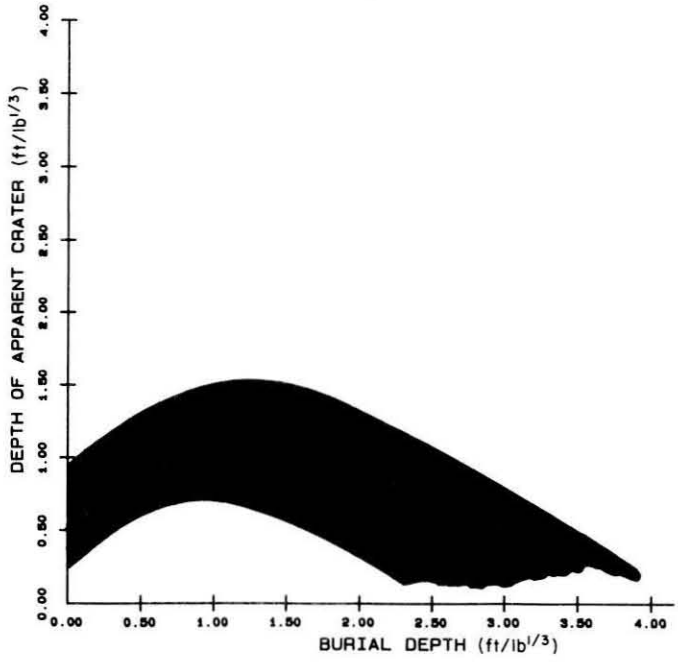

b. Scaled crater depth as a function of scaled charge depth.

Figure 10. Summary of scaled dimensions for apparent craters in massive ice. (Data from Livingston 1960.)

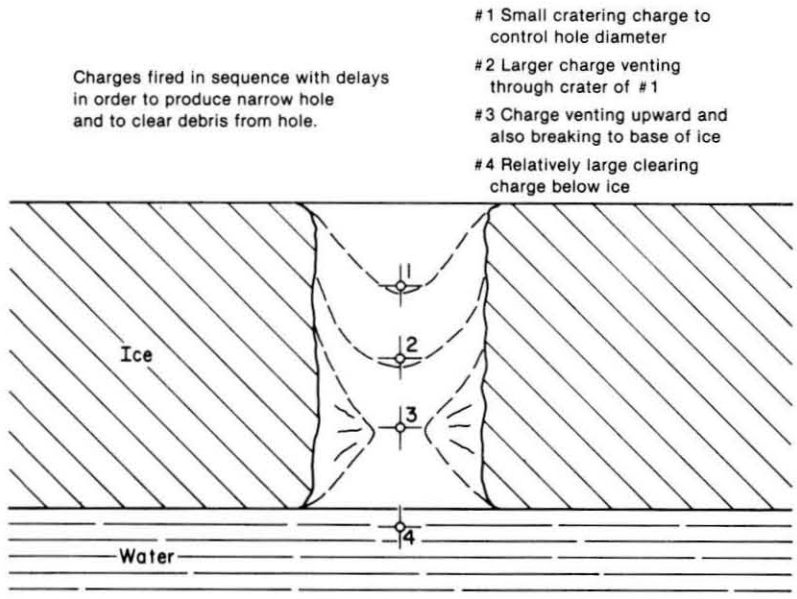

Figure 11. Use of delay deck charges to break a narrow shaft through very thick ice.

A charge set at, or below, mid-depth can break out to both the ice/air and the ice/water interfaces, provided that $t/2W^{1/3}$ is less than about 4 $ft/lb^{1/3}$ (1.6 $m/kg^{1/3}$). However, the maximum scaled radius of the upper or lower surface fracture zone is likely to drop below the 3 - 5 $ft/lb^{1/3}$ (1.2-2.0 $m/kg^{1/3}$) value for an optimum cratering charge in very thick ice.

To cut a relatively narrow vertical shaft through thick ice, delayed deck charges can be employed. Several charges are placed at different depths, and they are fired in rapid sequence, from top to bottom with appropriate delays (Fig. 11). The top charge is designed to produce the required hole diameter, in accordance with the cratering data of Figure 9. Successive charges vent through this crater, and a final charge in the water beneath the ice flushes out ice fragments (which unfortunately tend to wash back into the hole as water drains from the ice surface).

When a small unconfined charge is laid on top of thick ice it makes a superficial crater, with the dimensions given by Figures 9 and 10 for zero charge depth. The scaled radius of the true crater is 2-3 $ft/lb^{1/3}$ (0.8 - 1.2 $m/kg^{1/3}$) at the surface, but the depth is small, say 0.6 to 1.0 $ft/lb^{1/3}$ (0.24 to 0.4 $m/kg^{1/3}$). In order for a surface charge to break through to the bottom of the ice sheet and to form a penetration crater, as

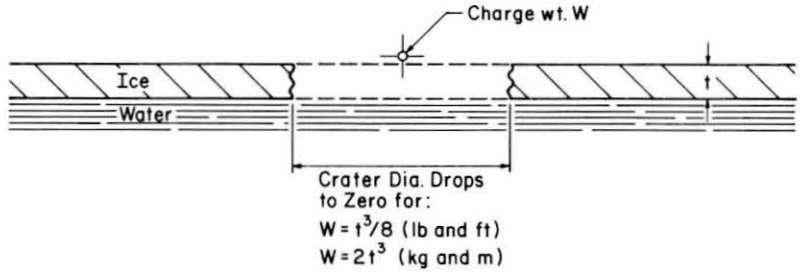

Figure 12. Effect of a charge lying on the upper surface of thin ice.

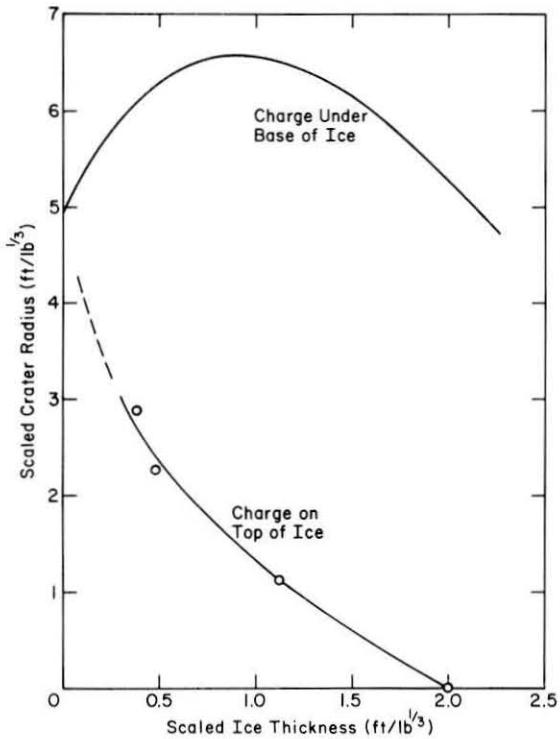

Figure 13. Effects of surface charges compared with the effects of under-ice charges. [Data for surface charges from Barash (1966) and Fonstad et al. (1982).]

in Figure 12, the scaled ice thickness has to be less than 2 ft/lb$^{1/3}$ (0.8 m/kg$^{1/3}$). As the scaled ice thickness decreases, the radius of the crater increases, but it is always much smaller than the radius of the crater that would be produced by the same charge set in water under the base of the ice sheet (Fig. 13). A surface charge is likely to produce more breakage if it is covered by sandbags or suchlike ("mudcapping" or "dobying").

A charge in air above the ice surface is even less effective than a surface charge. No systematic test results have been reported, but at a scaled ice thickness of 1 ft/lb$^{1/3}$ (0.4 m/kg$^{1/3}$), no crater is formed when the charge height is 0.5 ft/lb$^{1/3}$ (0.2 m/kg$^{1/3}$) or more.

Penetration by shaped charges

A shaped charge, or lined cavity charge, forms a high velocity jet and incorporates into it dense material from a metal or glass cavity liner. Typical charges, which are rotationally symmetrical, produce a narrow hole in the target material. There are also linear shaped charges, which produce a slot in the target.

Some guidelines for ice penetration by typical shaped charges with conical liners have been developed (Mellor 1984b), although test results are few. Depending on the cone angle of the charge, penetration depth in thick ice is likely to be in the range 12 to 16 cone diameters, with mean hole diameter in the range 1/3 to 2/3 of the cone diameter. Deep penetration (16 cone diameters) and a slender hole (1/3 cone diameter) are likely to be achieved with narrow cone angles, say around 45°. Smaller penetration (12 cone diameters) and a wider hole are likely with wide-angle cones (> 60°). Optimum standoff distance is likely to be in the range 2 to 4 cone diameters, depending somewhat on cone angle. All of these values are for a shaped charge detonating in air above the ice (Fig. 14).

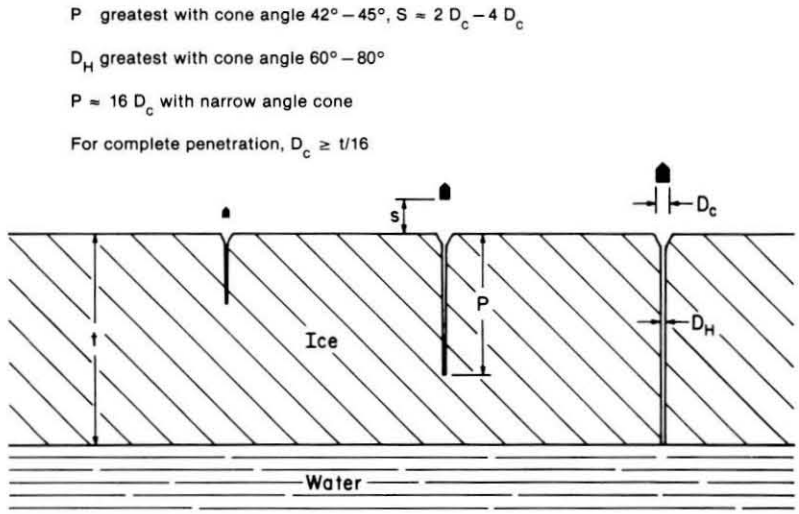

Figure 14. Effect of conventional shaped charges fired into the top surface of an ice sheet.

A shaped charge fired underwater needs a standoff cavity where the jet can develop before it strikes the target material. This can be a canister filled with air or with low-density foamed plastic. Penetration by the explosive jet should then be similar to the penetration from air, but containment of the charge by water could lead to greater local cratering in the ice surface.

Conclusion

Empirical prediction curves for explosive ice-breaking have been developed in various forms from test data, using regression analysis. The "standard" form given in Figure 1 is convenient for practical use, and it appears to represent the data slightly better than alternative forms, which may have somewhat closer relation to the relevant physics (Fig. 5 and 6).

There is still likely to be considerable error when the result of a particular blast is compared with the statistically based prediction. However, the present guidelines are an improvement over some earlier rules for ice blasting, which ignored ice thickness as a variable and gave optimum charge depth as an absolute value, irrespective of charge size.

The main requirement for improving prediction capability is more data from well-designed field tests, including tests with multiple charges, surface charges, charges above the ice, linear charges above and below the ice, and shaped charges above and below the ice. Test shots should include conditions that are far from optimum, and crater dimensions should be defined consistently.

Literature cited

Barash, R.M. (1966) Ice-breaking by explosives. U.S. Naval Ordnance Laboratory, NOLTR 66-229.

Fonstad, G.D., R. Gerard and B. Stimpson (1982) The explosive demolition of floating ice sheets. In POAC 81: Proceedings, Sixth International Conference on Port and Ocean Engineering Under Arctic Conditions, Laval University, Quebec City, Quebec, Canada, Volume II.

Fonstad, G.D. and R. Gerard (1985) Field tests of techniques for explosive cratering of floating ice sheets. Proceedings of Annual Conference, Canadian Society for Civil Engineering, Saskatoon, Saskatchewan.

Kurtz, M.K., R.H. Benfer, W.G. Christopher, G.E. Frankenstein, G. Van Wyhe and E.A. Roguski (1966) Consolidated report, Operation Break-up, FY 66. Ice cratering experiments, Blair Lake, Alaska. Nuclear Cratering Group, Lawrence Radiation Laboratory, Livermore, California, NCG/TM 66-7.

Leslie, D.M. and C.A. Nelson (1961) Explosion tests under thick polar ice. U.S. Naval Ordnance Laboratory, NOLTR 61-146.

Livingston, C.W. (1960) Explosions in ice. USA Snow, Ice and Permafrost Research Establishment, Technical Report 75.

Mellor, M. (1972) Data for ice blasting. USA Cold Regions Research and Engineering Laboratory, Technical Note (unpublished).

Mellor, M. (1982) Breaking ice with explosives. USA Cold Regions Research and Engineering Laboratory, CRREL Report 82-40.

Mellor, M. (1984a) Icebreaking by gas blasting. IAHR Ice Symposium, Hamburg.

Mellor, M. (1984b) Penetration of shaped charges into ice. In Workshop on Ice Penetration Technology (W.F. Weeks and M. Kleinerman, Ed.), USA Cold Regions Research and Engineering Laboratory, Special Report 84-33 (limited distribution).

Mellor, M. (1986) Blasting and blast effects in cold regions, Part II: Underwater explosions, USA Cold Regions Research and Engineering Laboratory, Special Report 86-16

APPENDIX A: TEST DATA ADDED TO THE FILE SINCE PREVIOUS REPORT (MELLOR 1982)

Table A1. Project Ice Skate, Bering Sea, February 1960. U.S. Naval Ordnance Laboratory (now U.S. Naval Surface Weapons Center)*. Explosive: HBX-3.

Charge weight (lb)	Average ice thickness (ft)	Depth of charge below base of ice (ft)	Average crater diameter (ft)
630	4.6	30	100
630	2.3	20	110
630	2.6	45	90

*Leslie and Nelson (1961). Data and report provided by courtesy of Robert M. Barash, Explosion Damage Branch, USNSWC.

Table A2. Polar Ice Experiment, Beaufort Sea, Summer 1961. U.S. Naval Ordnance Laboratory (now U.S. Naval Surface Weapons Center)*. Explosive: HBX-3.

Charge weight (lb)	Average ice thickness (ft)	Depth of charge below base of ice (ft)	Average crater diameter (ft)
60	10	3.91	100
35	14	3.27	40
20	9.3	2.71	0

*Leslie and Nelson (1961). Data and report provided by courtesy of Robert M. Barash, Explosion Damage Branch, USNSWC.

Table A3. Tests by M. Mellor, Imjin River, Korea, February 1983. Water depth: 20 ft (6 m); explosive: C-4.

Charge weight (lb)	Charge weight (kg)	Charge depth (ft)	Charge depth (m)	Ice thickness (in)	Ice thickness (m)	Crater diameter (ft)	Crater diameter (m)
1.25	0.567	8	2.44	4.25	0.11	3.5	1.07
1.25	0.567	10	3.05	3	0.08	5.6	1.71
1.25	0.567	12	3.66	4.25	0.11	3.5	1.07
1.25	0.567	5	1.52	4	0.10	7.3	2.22
1.25	0.567	14	4.27	4	0.10	0	0
1.25	0.567	2	0.61	6	0.15	13.7	4.18
1.25	0.567	0	0	6	0.15	13.3	4.05
3.75	1.70	14	4.27	6	0.15	0	0
2.5	1.13	10	3.05	4	0.10	0	0

Table A4. Tests by M. Mellor at Bolt Technology test site, January 1984. Explosive: AN + NM binary

Charge weight (lb)	Charge depth below base of ice (ft)	Ice thickness (in)	Crater diameter (ft)
0.667	5	11	3
1.333	5	11	5
0.667	0	12	9.5
1.333	0	12	13.0
1.333	2.5	12	13.7
2.9	4	12	14

Table A5. Tests made on Imjin River, Korea, by E Company, 2nd Engineer Battalion, U.S. Army (these results not included in analysis).

Explosive	Charge weight (lb)	Charge depth below base of ice (ft)	Ice thickness (in)	Crater diameter (ft)
C4	1.25	0.33	9	18
Military dynamite	1.0	0.33	11.25	8
C4	2.5	0.33	11	20

Table A6. Pattern shot on Imjin River, Korea, by E Company, 2nd Engineer Battalion, U.S. Army (data recorded by D. Calkins, CRREL, January 1986.)

Explosive
C4

Weight of single charge
1.25 lb (2.5 lb in center row)

Ice thickness (average)
0.89 ft

R_{c1}
6.52 ft/lb$^{1/3}$

s/R_{c1}
2.76

Water depth
6 - 8 ft

Charge depth
0.33 ft

Pattern
Square mesh, 5 rows 18 ft apart, 16 charges per row at 18-ft centers

Fragmentation
Equant fragments in central crater zones, some small slabs near midpoints of charge net.

APPENDIX B: CURRENT DATA FILE

Test data are tabulated in the following columns:

X_1 - charge depth below base of ice sheet ($ft/lb^{1/3}$)

X_2 - ice thickness ($in./lb^{1/3}$)

X_3 - ice thickness ($ft/lb^{1/3}$)

X_4 - water level to base of ice ($ft/lb^{1/3}$)

X_5 - charge depth below water level ($ft/lb^{1/3}$)

X_6 - charge weight (lb)

X_7 - theoretical maximum bubble radius during first pulse ($ft/lb^{1/3}$)

X_8 - charge depth below water level scaled with respect to X_7

X_9 - ice thickness scaled with respect to X_7

Y_1 - crater radius ($ft/lb^{1/3}$)

Y_2 - crater radius scaled with respect to maximum bubble radius, X_7

The actual measured values are scaled and entered as Y_1, X_1 and X_2/X_3. The charge weight is listed as X_6. All other quantities are generated from these values.

X1	X2	X3	X4	X5	X6	X7	X8	X9	Y1	Y2
4.00	19.2	1.60	1.46	5.46	0.551	3.92	1.39	0.408	2.30	0.585
0.000	16.9	1.40	1.28	1.28	0.551	4.05	0.315	0.347	5.00	1.23
0.000	13.8	1.15	1.04	1.04	1.10	4.05	0.257	0.283	5.48	1.35
0.000	11.8	0.983	0.895	0.895	2.20	4.05	0.221	0.243	5.80	1.43
0.000	8.41	0.701	0.638	0.638	4.41	4.05	0.157	0.173	6.15	1.52
0.000	13.2	1.10	0.999	0.999	0.551	4.06	0.246	0.270	4.81	1.18
0.000	10.5	0.872	0.794	0.794	1.10	4.06	0.195	0.215	6.20	1.53
0.000	10.5	0.872	0.794	0.794	1.10	4.06	0.195	0.215	6.20	1.53
0.000	8.30	0.692	0.629	0.629	2.20	4.06	0.155	0.170	6.69	1.65
3.33	5.93	0.494	0.450	3.78	18.7	3.75	1.01	0.132	5.88	1.57
6.36	15.3	1.27	1.16	7.52	1.10	3.82	1.97	0.334	1.27	0.333
5.05	12.1	1.01	0.919	5.97	2.20	3.82	1.56	0.265	1.25	0.330
4.00	9.60	0.800	0.728	4.73	4.41	3.82	1.24	0.210	6.00	1.57
3.53	8.48	0.706	0.637	4.14	6.62	3.82	1.08	0.183	6.13	1.61
1.85	4.07	0.339	0.309	2.16	18.7	3.89	0.556	0.879E-01	6.43	1.67
3.18	15.3	1.27	1.16	4.34	1.10	3.92	1.11	0.324	6.68	1.70
2.52	12.1	1.01	0.919	3.44	2.20	3.92	0.876	0.257	7.92	2.02
2.00	9.60	0.800	0.728	2.73	4.41	3.92	0.695	0.204	7.01	1.79
1.75	8.40	0.700	0.637	2.39	6.62	3.92	0.608	0.178	8.11	2.07
1.59	10.5	0.872	0.794	2.38	1.10	4.00	0.596	0.218	6.20	1.55
1.26	8.30	0.692	0.629	1.89	2.20	4.00	0.473	0.173	6.17	1.54
1.00	6.58	0.548	0.499	1.50	4.41	4.00	0.375	0.137	6.00	1.50
1.23	25.1	2.42	2.21	3.44	0.618	3.98	0.863	0.609	4.62	1.16
1.23	25.1	2.42	2.21	3.44	0.618	3.98	0.863	0.609	4.62	1.16
1.65	24.0	2.00	1.82	3.48	0.618	3.98	0.874	0.504	4.81	1.21
1.84	21.7	1.81	1.65	3.49	0.618	3.98	0.876	0.455	5.48	1.39
1.84	21.7	1.81	1.65	3.49	0.618	3.98	0.876	0.455	5.48	1.38
0.000	43.9	3.66	3.33	3.33	0.618	3.98	0.836	0.918	4.25	1.07
0.000	43.9	3.66	3.33	3.33	0.618	3.98	0.836	0.918	4.25	1.07
0.981	23.2	1.93	1.76	2.74	1.23	3.98	0.689	0.486	6.13	1.54
0.981	23.2	1.93	1.76	2.74	1.23	3.98	0.689	0.486	6.13	1.54
1.32	19.1	1.60	1.45	2.77	1.23	3.98	0.697	0.401	5.82	1.46
1.47	17.3	1.44	1.31	2.78	1.23	3.98	0.699	0.362	5.49	1.38
1.47	17.3	1.44	1.31	2.78	1.23	3.98	0.699	0.362	5.49	1.38
1.25	20.1	1.66	1.53	2.78	1.85	3.96	0.701	0.424	5.33	1.35
1.54	16.7	1.39	1.26	2.81	1.85	3.96	0.709	0.350	6.66	1.68
1.67	15.0	1.25	1.14	2.81	1.85	3.96	0.711	0.316	6.66	1.68
0.000	3.54	0.295	0.268	0.268	1.00	4.08	0.657E-01	0.722E-01	5.00	1.22
1.64	4.33	0.361	0.328	1.97	1.00	4.02	0.490	0.898E-01	5.58	1.39
0.000	3.13	0.260	0.237	0.237	2.00	4.08	0.580E-01	0.638E-01	5.49	1.34
1.33	4.37	0.364	0.331	1.63	2.00	4.01	0.407	0.907E-01	5.47	1.36
5.21	4.07	0.339	0.309	5.52	2.00	3.84	1.44	0.883E-01	3.26	0.849
1.65	3.95	0.330	0.300	1.95	15.4	3.91	0.499	0.843E-01	3.30	0.844
1.65	3.95	0.330	0.300	1.95	15.4	3.91	0.499	0.843E-01	3.30	0.844
1.95	3.95	0.330	0.300	2.25	26.5	3.85	0.585	0.856E-01	4.46	1.16
1.95	3.95	0.330	0.300	2.25	26.5	3.85	0.585	0.856E-01	4.46	1.16
1.84	4.69	0.391	0.356	2.20	26.5	3.85	0.570	0.101	3.91	1.01
1.84	4.69	0.391	0.356	2.20	26.5	3.85	0.570	0.101	3.91	1.01
2.20	4.31	0.359	0.327	2.53	33.1	3.80	0.664	0.944E-01	3.84	1.01
2.20	4.31	0.359	0.327	2.53	33.1	3.80	0.664	0.944E-01	3.84	1.01
1.86	3.63	0.302	0.275	2.14	55.1	3.80	0.561	0.795E-01	5.18	1.35
1.86	3.63	0.302	0.275	2.14	55.1	3.80	0.561	0.795E-01	5.18	1.36
1.73	6.02	0.502	0.456	2.19	26.5	3.86	0.567	0.130	3.35	0.869
1.73	6.02	0.502	0.456	2.19	26.5	3.86	0.567	0.130	3.35	0.869
1.77	4.66	0.388	0.353	2.12	55.1	3.81	0.558	0.102	6.06	1.59
1.77	4.66	0.388	0.353	2.12	55.1	3.81	0.558	0.102	6.06	1.59
1.62	7.38	0.615	0.560	2.18	26.5	3.86	0.565	0.160	3.91	1.01
1.62	7.38	0.615	0.560	2.18	26.5	3.86	0.565	0.160	3.91	1.01
1.68	5.71	0.476	0.433	2.11	55.1	3.81	0.555	0.125	6.06	1.59
1.68	5.71	0.476	0.433	2.11	55.1	3.81	0.555	0.125	6.06	1.59
1.56	8.71	0.726	0.660	2.16	26.5	3.86	0.560	0.188	3.91	1.01
1.56	8.71	0.726	0.660	2.16	26.5	3.86	0.560	0.188	3.91	1.01
1.60	6.73	0.561	0.510	2.11	55.1	3.81	0.554	0.147	5.19	1.36
1.60	6.73	0.561	0.510	2.11	55.1	3.81	0.554	0.147	5.19	1.36
0.520	19.7	1.64	1.49	2.01	55.1	3.82	0.527	0.430	3.55	0.959
0.520	19.7	1.64	1.49	2.01	55.1	3.82	0.527	0.430	3.66	0.959
1.58	3.35	0.279	0.254	1.83	5.51	3.97	0.462	0.703E-01	6.97	1.76
1.58	3.35	0.279	0.254	1.83	5.51	3.97	0.462	0.703E-01	6.97	1.76
0.464	5.58	0.465	0.423	0.887	5.51	4.03	0.220	0.115	6.52	1.62
0.464	5.58	0.465	0.423	0.887	5.51	4.03	0.220	0.115	6.52	1.62
0.368	4.40	0.367	0.334	0.700	11.2	4.03	0.174	0.909E-01	5.49	1.36
0.368	4.40	0.367	0.334	0.700	11.2	4.03	0.174	0.909E-01	5.49	1.36
0.368	4.40	0.367	0.334	0.700	11.2	4.03	0.174	0.909E-01	5.49	1.36
2.56	4.40	0.367	0.334	2.89	11.2	3.86	0.750	0.951E-01	6.21	1.61
2.56	4.40	0.367	0.334	2.89	11.2	3.86	0.750	0.951E-01	6.21	1.61
2.56	4.40	0.367	0.334	2.89	11.2	3.86	0.750	0.951E-01	6.21	1.61
1.21	7.82	0.652	0.593	1.80	5.51	3.97	0.453	0.164	7.43	1.87
1.21	7.82	0.652	0.593	1.80	5.51	3.97	0.453	0.164	7.43	1.87
1.21	7.82	0.652	0.593	1.80	5.51	3.97	0.453	0.164	7.43	1.87

X1	X2	X3	X4	X5	X6	X7	X8	X9	Y1	Y2
1.21	7.32	0.652	0.593	1.80	5.51	3.97	0.453	0.164	7.43	1.87
1.21	7.32	0.652	0.593	1.80	5.51	3.97	0.453	0.164	7.43	1.87
2.42	5.16	0.513	0.467	2.89	11.2	3.86	0.749	0.133	6.58	1.71
2.42	5.16	0.513	0.467	2.89	11.2	3.86	0.749	0.133	6.58	1.71
1.21	16.0	0.833	0.758	1.78	5.51	3.97	0.448	0.210	7.43	1.87
1.21	16.0	0.833	0.758	1.78	5.51	3.97	0.448	0.210	7.43	1.87
1.21	16.0	0.833	0.758	1.78	5.51	3.97	0.448	0.210	7.43	1.87
1.21	16.0	0.833	0.758	1.78	5.51	3.97	0.448	0.210	7.43	1.87
1.21	12.2	1.02	0.927	1.76	5.51	3.97	0.444	0.257	6.04	1.52
1.21	12.2	1.02	0.927	1.76	5.51	3.97	0.444	0.257	6.04	1.52
1.21	12.2	1.02	0.927	1.76	5.51	3.97	0.444	0.257	6.04	1.52
1.21	14.5	1.21	1.10	1.75	5.51	3.97	0.441	0.304	6.52	1.64
1.21	14.5	1.21	1.10	1.75	5.51	3.97	0.441	0.304	6.52	1.64
1.21	14.5	1.21	1.10	1.75	5.51	3.97	0.441	0.304	6.52	1.64
1.57	18.9	1.57	1.43	1.71	5.51	3.98	0.430	0.396	4.33	1.23
1.57	18.9	1.57	1.43	1.71	5.51	3.98	0.430	0.396	4.88	1.23
0.329	3.95	0.329	0.300	7.50	90.0	3.26	2.30	0.191	5.80	1.78
0.387	4.64	0.387	0.352	3.60	90.0	3.60	1.00	0.127	3.48	0.967
0.329	3.95	0.329	0.300	1.69	90.0	3.83	0.441	0.859E-01	6.95	1.82
0.309	3.71	0.309	0.281	2.37	90.0	3.74	0.634	0.826E-01	3.48	0.930
0.309	3.71	0.309	0.281	2.37	90.0	3.74	0.634	0.826E-01	3.48	0.930
0.309	3.71	0.309	0.281	2.37	90.0	3.74	0.634	0.826E-01	3.43	0.930
0.414	4.97	0.414	0.377	3.89	90.0	3.66	1.06	0.113	7.31	2.00
0.557	6.68	0.557	0.507	0.507	137.	3.99	0.127	0.139	6.58	1.65
0.545	6.54	0.545	0.496	1.47	135.	3.82	0.384	0.143	6.56	1.72
0.590	7.08	0.590	0.537	2.52	136.	3.67	0.686	0.161	7.23	1.95
0.565	6.78	0.565	0.514	3.39	142.	3.55	0.957	0.159	6.78	1.91
0.521	6.25	0.521	0.474	4.42	130.	3.44	1.28	0.151	3.76	1.09
0.493	5.92	0.493	0.449	5.24	142.	3.35	1.57	0.147	4.54	1.39
0.533	6.40	0.533	0.485	1.94	138.	3.75	0.516	0.142	6.92	1.85
0.528	6.34	0.528	0.481	7.44	128.	3.18	2.34	0.166	4.54	1.43
0.519	6.23	0.519	0.472	2.44	131.	3.68	0.664	0.141	5.96	1.62
0.527	6.32	0.527	0.479	2.41	140.	3.68	0.655	0.143	6.75	1.84
0.504	6.05	0.504	0.459	3.39	135.	3.55	0.953	0.142	5.14	1.45
0.529	6.35	0.529	0.482	4.42	131.	3.44	1.28	0.154	3.04	0.883
0.511	6.13	0.511	0.465	2.41	135.	3.68	0.656	0.139	6.91	1.88
0.500	6.00	0.500	0.455	4.28	143.	3.44	1.24	0.145	3.60	1.05
0.578	6.94	0.578	0.526	6.30	141.	3.25	1.94	0.178	1.63	0.501
0.293	3.52	0.293	0.267	2.21	140.	3.46	0.638	0.648E-01	8.54	2.47
0.429	5.15	0.429	0.391	6.85	160.	3.18	2.15	0.135	4.37	1.37
0.455	5.46	0.455	0.414	4.18	156.	3.45	1.21	0.132	5.09	1.48
0.442	5.30	0.442	0.402	3.39	50.0	3.68	0.922	0.120	5.76	1.57
0.442	5.30	0.442	0.402	3.25	50.0	3.69	0.881	0.120	5.45	1.48
0.466	5.59	0.466	0.424	3.52	33.3	3.71	0.950	0.126	4.97	1.34
0.243	2.92	0.243	0.221	6.07	5.00	3.74	1.62	0.651E-01	2.92	0.781
0.243	2.92	0.243	0.221	3.14	5.00	3.89	0.807	0.625E-01	4.68	1.20
0.243	2.92	0.243	0.221	1.39	5.00	4.00	0.348	0.608E-01	6.44	1.51
0.243	2.92	0.243	0.221	0.221	5.00	4.08	0.543E-01	0.596E-01	8.78	2.15
0.567	7.05	0.567	0.535	1.25	42.0	3.93	0.319	0.150	7.05	1.79
0.672	8.06	0.672	0.611	1.68	42.0	3.88	0.434	0.173	7.40	1.91
0.576	6.91	0.576	0.524	1.96	42.0	3.85	0.510	0.150	7.05	1.83
0.707	8.49	0.707	0.644	2.08	42.0	3.83	0.543	0.185	8.76	2.29
0.719	8.63	0.719	0.654	2.38	42.0	3.80	0.626	0.189	7.61	2.00
0.707	8.49	0.707	0.644	2.94	42.0	3.74	0.787	0.189	7.53	2.06
0.600	7.20	0.600	0.546	3.42	42.0	3.69	0.926	0.162	7.47	2.02
0.600	7.20	0.600	0.546	5.51	42.0	3.51	1.57	0.171	6.04	1.72
1.04	12.5	1.04	0.948	0.948	8.00	4.02	0.236	0.259	6.25	1.56
1.08	13.0	1.08	0.986	1.12	8.00	4.01	0.280	0.270	5.83	1.47
1.04	12.5	1.04	0.948	1.67	8.00	3.96	0.422	0.263	8.13	2.05
1.08	13.0	1.08	0.986	1.71	8.00	3.96	0.432	0.273	8.13	2.05
0.938	11.3	0.938	0.853	2.30	8.00	3.92	0.588	0.239	8.50	2.17
1.21	14.5	1.21	1.10	2.55	8.00	3.90	0.653	0.310	10.3	2.63
1.02	12.3	1.02	0.929	2.93	8.00	3.88	0.755	0.263	7.87	2.03
0.958	11.5	0.958	0.872	3.37	8.00	3.85	0.876	0.249	7.00	1.82
1.06	12.8	1.06	0.967	3.47	8.00	3.84	0.902	0.277	6.83	1.79
1.21	14.5	1.21	1.10	4.85	8.00	3.76	1.29	0.322	3.81	1.01
0.833	10.0	0.833	0.758	5.76	8.00	3.70	1.55	0.225	3.81	1.03
0.833	10.0	0.833	0.758	5.76	8.00	3.70	1.55	0.225	4.50	1.21
1.21	14.5	1.21	1.10	7.60	8.00	3.61	2.11	0.335	4.50	1.25
1.17	14.0	1.17	1.06	9.06	8.00	3.54	2.56	0.330	4.44	1.26
1.13	13.5	1.13	1.02	11.0	8.00	3.45	3.20	0.326	2.62	0.759
1.21	14.5	1.21	1.10	11.1	8.00	3.45	3.22	0.351	5.94	1.72
1.88	22.5	1.88	1.71	1.71	1.00	4.03	0.424	0.466	6.50	1.61
2.08	25.0	2.08	1.90	3.35	1.00	3.96	0.844	0.525	8.00	2.02
2.50	30.0	2.50	2.27	3.72	1.00	3.95	0.943	0.633	3.50	0.986
1.83	22.0	1.83	1.67	4.17	1.00	3.94	1.06	0.466	1.75	0.445
2.42	29.0	2.42	2.20	4.70	1.00	3.92	1.20	0.617	3.00	0.766
2.50	30.0	2.50	2.27	6.27	1.00	3.86	1.62	0.647	1.88	0.485
1.92	23.0	1.92	1.74	6.74	1.00	3.85	1.75	0.498	3.50	0.910
1.92	23.0	1.92	1.74	6.74	1.00	3.85	1.75	0.498	4.00	1.04

X1	X2	X3	X4	X5	X6	X7	X8	X9	Y1	Y2
5.00	26.0	2.17	1.97	6.97	1.00	3.84	1.82	0.564	1.50	0.391
5.66	32.0	2.50	2.27	7.27	1.00	3.83	1.90	0.653	0.875	0.228
6.00	30.0	2.50	2.27	8.27	1.00	3.80	2.18	0.658	2.25	0.592
7.50	29.0	2.42	2.20	9.70	1.00	3.76	2.58	0.643	0.750	0.200
10.00	27.0	2.25	2.05	12.0	1.00	3.69	3.27	0.610	0.000	0.000
11.00	24.0	2.42	2.20	13.2	1.00	3.66	3.61	0.661	0.000	0.000
0.000	16.0	1.33	1.21	1.21	1.00	4.05	0.300	0.330	5.35	1.45
1.50	19.0	1.58	1.44	2.94	1.00	3.98	0.739	0.398	7.25	1.82
3.00	17.0	1.42	1.29	4.29	1.00	3.93	1.09	0.360	8.50	2.16
4.50	19.0	1.58	1.44	5.94	1.00	3.87	1.53	0.409	2.05	0.529
1.59	25.8	2.15	1.96	3.55	2.00	3.92	0.904	0.548	3.97	1.01
1.58	22.5	1.71	1.55	3.13	4.00	3.91	0.802	0.437	2.84	0.727
0.000	21.4	1.78	1.62	1.62	3.50	4.00	0.406	0.446	3.29	0.823
2.48	17.3	1.45	1.32	3.80	0.500	3.98	0.954	0.364	6.71	1.59
1.97	13.8	1.15	1.04	3.01	1.00	3.98	0.758	0.289	6.15	1.55
1.45	10.2	0.847	0.770	2.22	2.50	3.98	0.558	0.213	7.86	1.98
1.15	8.06	0.672	0.611	1.76	5.00	3.98	0.443	0.169	7.20	1.81
8.00	5.50	0.458	0.417	8.42	1.00	3.79	2.22	0.121	4.00	1.05
4.00	5.00	0.417	0.379	4.38	1.00	3.93	1.11	0.106	6.65	1.69
2.00	5.10	0.425	0.387	2.39	1.00	4.00	0.597	0.106	5.55	1.39
0.000	5.50	0.458	0.417	0.417	1.00	4.08	0.102	0.112	5.75	1.41
6.08	2.44	0.203	0.185	6.26	10.0	3.65	1.72	0.557E-01	4.07	1.11
0.000	2.21	0.184	0.168	0.168	10.0	4.08	0.411E-01	0.451E-01	4.91	1.20
1.86	2.39	0.174	0.158	2.02	10.0	3.93	0.514	0.443E-01	5.37	1.37
3.71	2.21	0.184	0.168	3.88	10.0	3.80	1.02	0.485E-01	5.41	1.42
5.78	2.12	0.177	0.161	5.94	20.0	3.58	1.66	0.493E-01	4.17	1.16
2.95	2.21	0.184	0.168	3.12	20.0	3.79	0.822	0.485E-01	5.50	1.45
1.47	2.21	0.184	0.168	1.64	20.0	3.93	0.417	0.469E-01	5.32	1.36
0.000	2.21	0.184	0.168	0.168	20.0	4.08	0.411E-01	0.452E-01	5.38	1.32
9.44	6.52	0.543	0.494	9.98	0.600	3.79	2.63	0.143	0.000	0.000
4.74	6.52	0.543	0.494	5.23	0.600	3.93	1.33	0.138	1.33	0.339
2.37	6.52	0.543	0.494	2.86	0.600	4.00	0.716	0.136	6.12	1.53
0.000	7.11	0.592	0.539	0.539	0.600	4.08	0.132	0.145	4.77	1.17
6.00	2.50	0.208	0.190	6.19	8.00	3.68	1.68	0.566E-01	2.56	0.696
7.56	3.78	0.315	0.287	7.85	4.00	3.68	2.13	0.856E-01	0.000	0.000
9.52	4.76	0.397	0.361	9.88	2.00	3.68	2.69	0.108	0.000	0.000
12.0	5.75	0.479	0.436	12.4	1.00	3.68	3.38	0.130	0.000	0.000
0.000	2.50	0.208	0.190	0.190	8.00	4.08	0.465E-01	0.511E-01	5.25	1.29
0.000	3.15	0.262	0.239	0.449	4.00	4.07	0.110	0.646E-01	4.55	1.14
0.000	3.97	0.331	0.301	0.301	2.00	4.08	0.738E-01	0.811E-01	5.15	1.26
1.75	1.68	0.140	0.127	1.88	40.0	3.86	0.487	0.363E-01	7.46	1.93
0.390	6.22	0.518	0.472	0.862	0.600	4.07	0.212	0.128	5.04	1.24
0.480	13.3	1.11	1.01	1.49	2.20	4.02	0.370	0.275	7.35	1.96
0.300	10.5	0.878	0.799	1.10	4.41	4.02	0.273	0.218	8.12	2.02
0.280	9.55	0.796	0.724	1.00	2.76	4.04	0.249	0.197	6.53	1.62
0.300	9.97	0.831	0.756	1.06	2.76	4.04	0.262	0.206	6.90	1.71
0.000	12.1	1.01	0.919	0.919	1.10	4.06	0.227	0.249	6.99	1.72
0.000	9.22	0.768	0.699	0.699	2.20	4.06	0.172	0.189	5.82	1.43
0.000	7.92	0.660	0.601	0.601	4.96	4.05	0.148	0.163	6.27	1.55
0.000	6.52	0.543	0.494	0.494	9.92	4.05	0.122	0.134	6.40	1.58
0.000	12.6	1.05	0.954	0.954	1.10	4.05	0.235	0.259	7.50	1.85
0.000	11.5	0.960	0.874	0.874	2.20	4.05	0.216	0.237	6.58	1.63
0.000	7.04	0.587	0.534	0.534	4.96	4.06	0.132	0.145	5.75	1.42
0.000	5.59	0.466	0.424	0.424	9.92	4.06	0.104	0.115	6.44	1.59
0.000	12.3	1.03	0.936	0.936	1.10	4.06	0.231	0.254	5.02	1.24
0.000	11.5	0.960	0.874	0.874	2.20	4.05	0.216	0.237	5.54	1.37
0.000	8.35	0.696	0.633	0.633	4.96	4.05	0.156	0.172	6.14	1.52
0.000	6.87	0.572	0.521	0.521	9.92	4.05	0.129	0.141	6.90	1.70
0.500	14.5	1.21	1.10	1.10	1.10	4.05	0.272	0.299	6.67	1.65
0.000	11.5	0.960	0.874	0.874	2.20	4.05	0.216	0.237	6.55	1.62
0.000	8.22	0.685	0.623	0.623	4.96	4.05	0.154	0.169	7.25	1.79
0.000	6.98	0.582	0.529	0.529	9.92	4.05	0.131	0.144	6.92	1.71
0.440	14.5	1.21	1.10	1.54	1.10	4.03	0.382	0.300	5.65	1.40
0.280	9.62	0.802	0.729	1.01	2.20	4.04	0.250	0.198	5.32	1.44
0.230	7.92	0.660	0.601	0.831	4.96	4.04	0.206	0.163	6.62	1.64
0.180	6.05	0.504	0.459	0.639	9.92	4.04	0.158	0.125	5.86	1.45
0.350	12.1	1.01	0.919	1.27	1.10	4.04	0.314	0.250	6.10	1.51
0.280	9.22	0.768	0.699	0.979	2.20	4.04	0.242	0.190	6.50	1.61
0.230	9.37	0.781	0.711	1.00	4.96	4.03	0.248	0.194	6.48	1.61
0.210	6.98	0.582	0.529	0.739	9.92	4.03	0.183	0.144	6.52	1.62
0.410	14.0	1.17	1.06	1.47	1.10	4.03	0.365	0.290	6.07	1.50
0.350	11.5	0.960	0.874	1.22	2.20	4.03	0.304	0.238	6.05	1.50
0.270	8.79	0.732	0.667	0.937	4.96	4.03	0.232	0.182	6.27	1.56
0.210	7.09	0.591	0.538	0.748	9.92	4.03	0.185	0.147	6.05	1.50
0.440	14.5	1.21	1.10	1.54	1.10	4.03	0.382	0.300	5.72	1.42
0.350	11.5	0.960	0.874	1.22	2.20	4.03	0.304	0.238	7.51	1.86
0.270	8.79	0.732	0.667	0.937	4.96	4.03	0.232	0.182	6.75	1.67
0.200	6.52	0.543	0.494	0.694	9.92	4.03	0.172	0.135	7.10	1.75
2.22	12.8	1.07	0.974	3.19	1.10	3.97	0.805	0.270	5.91	1.46
1.74	9.98	0.832	0.757	2.50	2.20	3.97	0.629	0.210	6.63	1.67

X1	X2	X3	X4	X5	X6	X7	X8	X9	Y1	Y2
1.58	7.39	0.757	0.689	2.27	4.96	3.95	0.575	0.192	6.39	1.62
1.18	6.74	0.562	0.511	1.69	9.92	3.95	0.428	0.142	6.47	1.64
2.48	15.0	1.25	1.14	3.62	1.10	3.95	0.916	0.317	5.55	1.41
1.97	11.9	0.992	0.903	2.87	2.20	3.95	0.727	0.251	6.10	1.54
1.48	8.93	0.744	0.677	2.16	4.96	3.95	0.546	0.188	6.64	1.68
1.19	7.22	0.602	0.547	1.74	9.92	3.95	0.440	0.152	6.35	1.51
2.88	9.37	0.781	0.711	3.59	4.96	3.87	0.928	0.202	6.79	1.76
2.96	9.09	0.757	0.689	3.65	4.96	3.86	0.944	0.196	6.40	1.66
1.70	3.72	0.310	0.282	1.98	44.1	3.84	0.516	0.807E-01	5.81	1.51
1.47	3.80	0.317	0.288	1.76	55.1	3.85	0.457	0.823E-01	6.38	1.66
2.44	17.7	1.47	1.34	3.78	0.551	3.97	0.951	0.371	7.60	1.91
3.64	17.7	1.47	1.34	4.98	0.551	3.94	1.26	0.374	4.44	1.13
4.88	17.1	1.42	1.30	6.18	0.551	3.90	1.58	0.365	2.24	0.574
7.32	17.1	1.42	1.30	8.62	0.551	3.84	2.25	0.371	3.16	0.823
2.29	10.8	0.897	0.816	3.11	2.20	3.94	0.788	0.228	6.48	1.64
3.07	10.8	0.897	0.816	3.89	2.20	3.90	0.995	0.230	5.70	1.45
3.83	10.8	0.897	0.816	4.65	2.20	3.87	1.20	0.232	3.23	0.834
4.61	10.8	0.897	0.816	5.43	2.20	3.84	1.41	0.234	2.55	0.564
0.313	9.41	0.784	0.714	1.02	3.31	4.03	0.254	0.194	7.11	1.76
0.310	9.41	0.784	0.714	1.02	3.31	4.03	0.254	0.194	5.95	1.48
0.310	9.41	0.784	0.714	1.02	3.31	4.03	0.254	0.194	7.13	1.77
0.310	9.41	0.784	0.714	1.02	3.31	4.03	0.254	0.194	7.20	1.79
0.313	9.41	0.784	0.714	1.02	3.31	4.03	0.254	0.194	6.36	1.58
0.310	9.41	0.784	0.714	1.02	3.31	4.03	0.254	0.194	6.54	1.62
1.40	12.4	1.03	0.941	2.34	1.32	3.99	0.586	0.259	5.44	1.36
1.73	9.94	0.828	0.754	2.48	2.65	3.96	0.627	0.209	6.41	1.62
1.42	8.22	0.685	0.623	2.04	4.96	3.96	0.516	0.173	6.73	1.70
1.07	6.04	0.503	0.458	1.53	9.94	3.97	0.385	0.127	6.13	1.55
2.06	12.8	1.06	0.968	3.03	1.32	3.97	0.763	0.268	6.31	1.59
1.73	9.94	0.828	0.754	2.48	2.65	3.96	0.627	0.209	5.74	1.45
1.35	8.22	0.685	0.623	1.97	4.96	3.96	0.498	0.173	5.54	1.40
1.13	6.87	0.572	0.521	1.65	9.94	3.96	0.417	0.145	6.75	1.71
2.40	13.9	1.16	1.05	3.45	1.26	3.95	0.874	0.293	3.13	0.792
1.98	11.2	0.937	0.852	2.83	2.49	3.95	0.718	0.237	6.58	1.67
1.57	9.07	0.756	0.688	2.26	5.00	3.95	0.572	0.192	6.90	1.75
1.25	7.20	0.600	0.546	1.80	10.0	3.95	0.455	0.152	5.71	1.45
1.02	8.90	0.742	0.675	1.69	5.00	3.98	0.426	0.186	6.42	1.61
2.25	13.0	1.08	0.985	3.23	1.26	3.96	0.817	0.273	3.31	0.835
1.77	11.2	0.937	0.852	2.62	2.49	3.96	0.663	0.237	4.14	1.05
2.06	11.0	0.920	0.837	2.90	55.6	3.72	0.779	0.247	5.42	1.46
2.41	11.0	0.920	0.837	3.25	55.6	3.68	0.882	0.250	5.30	1.49
2.75	11.0	0.920	0.837	3.59	55.6	3.65	0.984	0.252	5.80	1.59
3.01	11.0	0.920	0.837	3.85	55.6	3.62	1.06	0.254	5.67	1.57
3.44	11.0	0.920	0.837	4.28	55.6	3.58	1.19	0.257	5.55	1.55
3.87	11.0	0.920	0.837	4.71	55.6	3.54	1.33	0.260	4.52	1.29
2.27	10.7	0.892	0.812	3.08	66.1	3.68	0.838	0.243	5.31	1.44
2.60	10.7	0.892	0.812	3.41	66.1	3.64	0.937	0.245	5.64	1.55
2.84	10.7	0.892	0.812	3.65	66.1	3.62	1.01	0.247	5.40	1.49
3.24	10.7	0.892	0.812	4.05	66.1	3.58	1.13	0.249	5.03	1.41
3.65	10.7	0.892	0.812	4.46	66.1	3.54	1.26	0.252	4.58	1.29
2.46	11.4	0.948	0.863	3.32	66.1	3.65	0.910	0.260	6.12	1.68
2.45	10.7	0.892	0.812	3.24	1.25	3.96	0.819	0.225	6.12	1.55
7.43	3.95	0.329	0.300	7.73	1.25	3.80	2.04	0.867E-01	1.62	0.427
9.28	2.78	0.232	0.211	9.49	1.25	3.74	2.54	0.619E-01	2.60	0.695
11.1	3.95	0.329	0.300	11.4	1.25	3.68	3.11	0.894E-01	1.62	0.440
4.64	3.71	0.309	0.281	4.92	1.25	3.90	1.26	0.794E-01	3.39	0.870
13.0	3.71	0.309	0.281	13.3	1.25	3.63	3.66	0.852E-01	0.000	0.000
1.86	5.57	0.464	0.422	2.28	1.25	4.00	0.571	0.116	6.36	1.59
0.000	5.57	0.464	0.422	0.422	1.25	4.08	0.104	0.114	6.17	1.51
9.01	3.86	0.322	0.293	9.30	3.75	3.63	2.57	0.887E-01	0.000	0.000
7.37	2.95	0.246	0.224	7.59	2.50	3.74	2.03	0.658E-01	0.000	0.000
3.50	6.44	0.537	0.488	3.99	630.	3.23	1.24	0.166	5.83	1.81
2.33	3.22	0.268	0.244	2.57	630.	3.45	0.746	0.777E-01	6.42	1.95
5.25	3.64	0.303	0.276	5.53	630.	3.04	1.82	0.997E-01	5.25	1.73
1.00	30.7	2.55	2.33	3.33	60.0	3.66	0.908	0.696	12.8	3.49
1.02	51.4	4.28	3.90	4.92	35.0	3.59	1.37	1.19	6.11	1.70
1.00	41.1	3.43	3.12	4.12	20.0	3.71	1.11	0.924	0.000	0.000
5.72	12.6	1.05	0.955	6.68	0.667	3.88	1.72	0.271	1.72	0.444
4.54	9.99	0.833	0.758	5.30	1.33	3.88	1.37	0.215	2.27	0.585
0.000	13.7	1.14	1.04	1.04	0.667	4.06	0.256	0.281	5.43	1.34
0.000	10.9	0.908	0.827	0.827	1.33	4.06	0.204	0.224	5.90	1.45
2.27	10.9	0.908	0.827	3.10	1.33	3.96	0.781	0.229	6.22	1.57
3.17	9.52	0.794	0.722	3.89	2.00	3.91	0.996	0.203	5.55	1.42